DIAGENESIS AND BURIAL HISTORY MODELING OF HETEROGENEOUS MARGINAL MARINE TO SHOREFACE PALEOCENE GLAUCONITIC SANDSTONES, TARANAKI BASIN, NEW ZEALAND

SEAN R. O'NEILL,[1] STUART J. JONES,[1] AND PETER J.J. KAMP[2]
[1]Department of Earth Sciences, Durham University, Durham DH1 3LE, U.K.
[2]School of Science, University of Waikato, Hamilton 3240, New Zealand
e-mail: sean.oneill@durham.ac.uk

ABSTRACT: Paleocene marginal marine to shoreface glauconitic sandstones (F-Sands) of the Farewell Formation from the Maui Field in Taranaki Basin, New Zealand, demonstrate a diagenetic evolution driven by major shifts in acidic pore-water composition, rate of burial, and clay-mineral authigenesis. Mechanical compaction is the principal porosity-reducing mechanism during the first 2500 m of burial of the F-Sands. Continued mechanical compaction with long-grain contacts, concavo-convex contacts, and deformed liable grains are common throughout the F-Sands. Late-stage flow of dissolved CO_2 in the pore fluids of the Farewell Formation is thought to have been generated from thermal decarboxylation of coaly source rocks. The circulation of these CO_2-rich fluids will have dissolved into undersaturated pore fluids and partially catalyzed dissolution of feldspar and quartz, producing ions for the precipitation of kaolinite and chlorite. Timing of the diagenetic reactions, as determined using paragenetic observations, fluid-inclusion analysis, and burial history modeling, suggests that the quartz cements formed at a late stage ($> 100°$C, corresponding to 0–7 Ma) and is consistent with the migration of hydrocarbons, and associated CO_2, into the F-Sand reservoir. Significant secondary porosity is generated through the dissolution of feldspar, which is preserved due to late-stage of occurrence at close to present-day maximum burial. Dissolved solutes in the F-Sands sandstones are being preferentially precipitated in interbedded and surrounding fine-grained heterolithic siltstone to very fine-grained sandstone beds, leading to enhanced heterogeneity and preservation of secondary porosity. This study provides an improved understanding for diagenetic reconstruction of marginal marine to shoreface facies.

INTRODUCTION

Paleocene fluvial to marginal marine arkosic sandstones beds of the Farewell Formation are an important proven hydrocarbon reservoir in Taranaki Basin, New Zealand (Fig. 1). The Paleocene sedimentary system grades northwestward from fluvial deposits in southern Taranaki Basin, including within the Manaia Graben (Fig. 1), into marginal marine to shoreface glauconitic sandstones in central parts of the basin (known as the F-Sands in Maui Field, this study and wider onshore Taranaki Peninsula; Fig. 2) and then into shelf-marine mudrocks north of Taranaki Peninsula (Fig. 3). The fluvial succession has lower reservoir quality than the glauconitic sandstone beds due to intercalated sandstone and mudstone facies and greater depths of burial (Martin et al. 1994; O'Neill et al. 2018). The glauconitic sandstone facies (F-Sands; Fig. 2) display good reservoir quality (av. 16.2 % porosity) (STOS 1993a, 1993b; Killops et al. 2009; Strogen 2011), being a major oil reservoir in the Maui Field (Fig. 4) and other smaller fields on the Western Platform (Tui, Amokura, and Pateke; Fig. 1). The reservoir quality of the Farewell Formation and F-Sand sandstones in Taranaki Basin is controlled mainly by grain-size variations and presence of kaolinite, which is often cited as the single most important cause of reservoir quality degradation across the Paleocene of Taranaki Basin (Martin et al. 1994; Smale et al. 1999; Pollock et al. 2003; Killops et al. 2009).

Fluvial Farewell Formation sandstone beds in the Kupe South Field (Fig. 1) contain a diagenetic mineral assemblage that documents major shifts in pore-water chemistry during their burial history (Martin et al. 1994; Higgs et al. 2013). The dissolution of terrigenous grains and carbonate cement by the flow of CO_2-rich fluids through sandstone beds is considered to have generated secondary porosity in various Paleocene and Eocene reservoirs, beneath Taranaki Peninsula, previously described by Schmidt and McDonald (1979), Seewald (2003), Higgs et al. (2013), and references therein. This process occurs in both clastic (Franks and Forester 1984; Lundegard and Land 1986; Higgs et al. 2013; Yuan et al. 2015a) and carbonate (Mazzullo and Harris 1992; Esteban and Taberner 2003) reservoirs. The dissolution of feldspar grains and the generation of significant secondary porosity in the F-Sands is discussed here in the context of hydrocarbon maturation, the flow of aggressive acidic CO_2-rich fluids, and the potential ingression of meteoric fluids.

Glauconite-rich sandstone units such as the F-Sands are particularly significant in siliciclastic shoreline systems, especially estuarine, barrier-bar, and shoreface environments (Dyson 1998). Their lateral extent is typically explained by the displacement of facies belts during marine transgression. Glauconitic sandstone beds in shoreline depositional systems can give those systems excellent reservoir quality (Winn 1994; Çağatay et al. 1996; Slot-Petersen et al. 1998). The deformity of glauconite grains relative to host terrigenous grains can provide an indication of the extent of mechanical compaction and hence a proxy measure of reservoir quality during drilling, including measurement-while-drilling (MWD) controlled geosteering (e.g., Schulz-Rojahn et al. 2003).
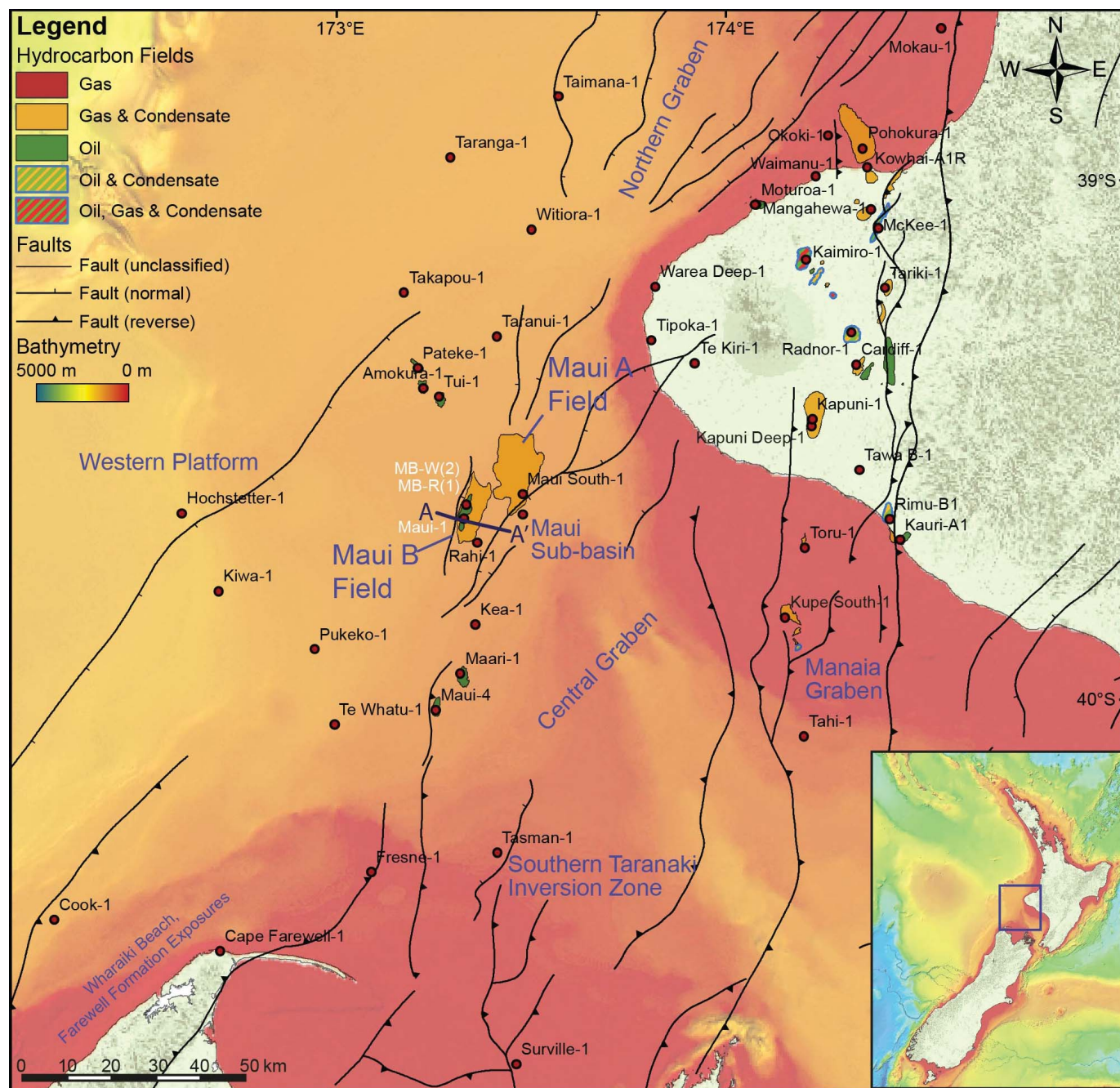
Fig. 1.—Map of Central and Southern Taranaki Basin showing the Maui Field, bathymetry, subsurface structure, and key wells. See Figure 4 for the line of cross section (A–A′) (bathymetry after Mitchell et al. 2012; faults and, fields after NZP&M 2014).

Here we present a diagenetic model for the Paleocene F-Sands of the Farewell Formation based on its depositional setting and its burial history at the Maui Field. In particular, we resolve the diagenetic paragenesis of the F-Sands for improved understanding of the mechanisms involved in the generation of secondary porosity, the precipitation of silica and clay cement, and the role played by heterogeneities of the sandstone facies.

GEOLOGICAL SETTING

Taranaki Basin covers approximately 100,000 km², mainly beneath the shelf and continental slope offshore of central-western North Island, New Zealand (Fig. 1). The only on-land sections of the basin occur beneath Taranaki Peninsula and northwesternmost South Island. The basin contains a Late Cretaceous to Quaternary sedimentary fill up to 8 km thick, as described by King and Thrasher (1996). The basin comprises a relatively undeformed block known as the Western Platform and a heavily deformed area termed the Eastern Mobile Belt (Fig. 1) (King and Thrasher 1996). The Eastern Mobile Belt contains significant shortening structures such as the Taranaki Fault (Fig.1), which defines the eastern margin of the basin along most of its length, and forms the locus of Miocene basement overthrusting westward into the basin (Stagpoole and Nicol 2008).
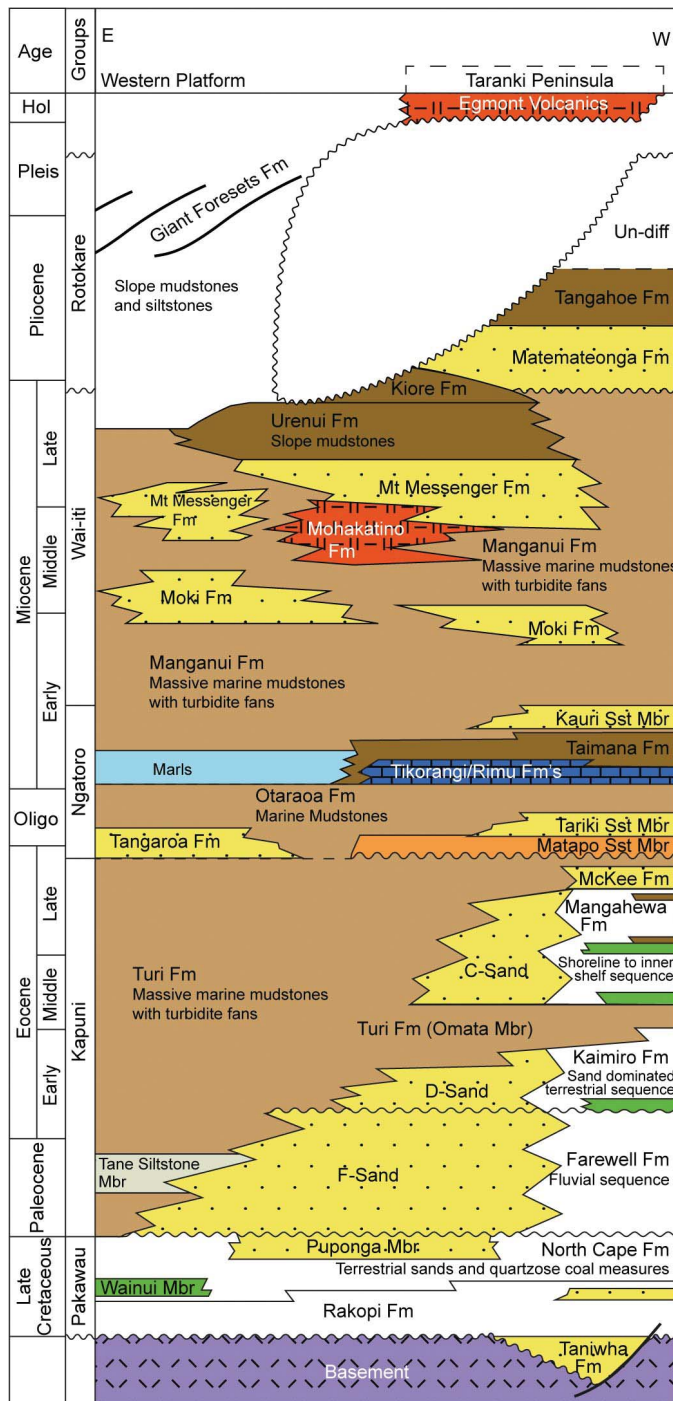
FIG. 2.—Subsurface stratigraphy of Taranaki Basin east to west from the Western Platform to Taranaki Peninsula (modified from King and Thrasher 1996).

The sedimentary fill of the Taranaki Basin records an early ($\sim$ 103–83 Ma) phase of extension, which is not well preserved in southern Taranaki Basin (Strogen et al. 2017) and a second phase at $\sim$ 84–57 Ma, concurrent with sea-floor spreading in the Tasman Sea to the west (King and Thrasher 1996). This extension has been attributed either to an intracontinental manifestation of a transform fault offsetting the spreading center, or to a failed-rift (Strogen et al. 2017). This extension resulted in the formation of normal fault-bounded grabens and half-grabens that became filled with

fluvial sandstone beds and intervening coal measures (Rakopi, North Cape, and Farewell formations; Fig. 2). From 52 Ma to $\sim$ 40 Ma the basin was tectonically quiescent, characterized by regional subsidence. The Paleocene to Eocene is characterized by overall transgression, with punctuated regressions, leading to the accumulation of well-sorted inner-shelf to fluvial sandstones (Fig. 3) capped by very fine-grained mudstones of the Omata Member and Turi Formation (Fig. 2). Fluvial sediments of the Paleocene and Eocene section (Farewell, Kaimiro, and Mangahewa formations; Fig. 2) contain the vast majority of the discovered hydrocarbon reserves in the Taranaki Basin, including the Maui Field (King and Thrasher 1996).

The early Oligocene (33–29 Ma) section is represented by minimal to no sediment accumulation in central and southern parts of the Taranaki Basin (Strogen et al. 2014b). This changed after $\sim$ 29 Ma with much higher rates of sediment accumulation in a foredeep that developed along the eastern margin of the basin (Stern and Davey 1990; Holt and Stern 1994) due to loading by basement across the Taranaki Fault (Tripathi and Kamp 2008). This was the expression in the Taranaki Basin of the early development of the modern Australia–Pacific plate boundary through New Zealand (Furlong and Kamp 2013). The Taranaki Fault at this time was a backthrust to the developing Hikurangi subduction zone offshore eastern North Island. Rapid subsidence of the foredeep led to bathyal conditions and proximal accumulation of a thick (800 m) calcareous mudstone succession (Otaraoa Formation; Fig. 2). By the latest Oligocene to earliest Miocene (25–22 Ma), shortening across the Taranaki Fault had resulted in a substantial basement high along the eastern basin margin, with shelfal bioclastic carbonate sediment forming upon it and being redeposited into the Taranaki Basin across a narrow shelf (Hood et al. 2003).

During the late Miocene–early Pliocene (from $\sim$ 12 Ma) crustal shortening in the southern Taranaki Basin and in the peninsula region, resulted in reactivation of Late Cretaceous normal faults as reverse faults, leading to the development or enhancement of positive structures (antiforms) and widespread inversion of the southern Taranaki Basin (Kamp and Green 1990; Crowhurst et al. 2002). These antiformal structures plunge northward and have been tested by exploration drilling. Southward, these structures emerge onshore in northern South Island, where shortening and inversion continued into the Pleistocene (King and Thrasher 1996; Vonk and Kamp 2008; Reilly et al. 2015; Bull et al. 2019), bringing Farewell Formation into outcrop close to Cape Farewell in northwestern South Island (Fig. 1).

The Maui Field

The Maui Field contains over three times more hydrocarbons than the second and third largest in the Taranaki Basin (Pohokura and Kapuni), and has been producing natural gas and condensate since 1979 (King and Thrasher 1996). The Maui Field is composed of two anticlinal closures that formed during the late Miocene–early Pliocene, bounded to the SE by the normal Cape Egmont Fault and to the SW by the Whitiki Fault (Fig. 4) (King and Thrasher 1996). The Maui High represents a pop-up structure, which formed through displacement on Whitiki Fault (Fig. 4) (Reilly et al. 2016). Hydrocarbons are trapped at multiple levels: in the Paleocene F-Sands (Farewell Formation), the Eocene C- and D-Sands (Mangahewa and Kaimiro formations), and the Miocene Moki Formation (Fig. 5) (Killops et al. 2009). Each of these reservoir units is capped by a mudrock section, and produce mainly gas, but oil rims are present in the C- and D-Sands and in the F-Sands on the Maui B structure (Seybold et al. 1996). The CO_2 content of the Maui Field gas, recorded from samples from across the field, is highly variable (av. 8.7%) but can reach a maximum of 21.5% (Funnell et al. 2001). The F-Sands are draped over a structural high on the Maui B structure (Fig. 4), thinning towards the northeast, producing oil until this reservoir was abandoned.
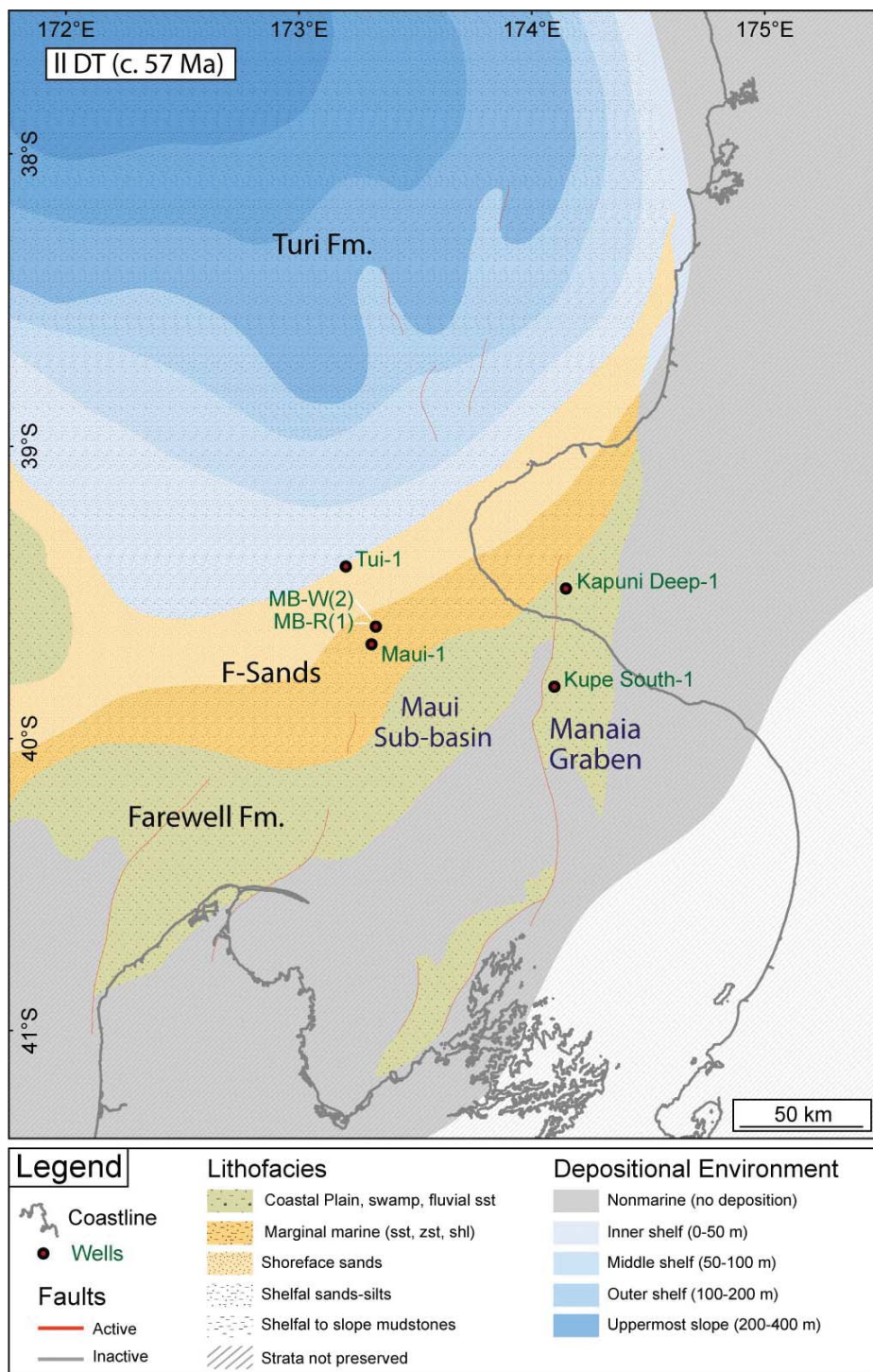
Fig. 3.—Paleogeographic map of Taranaki Basin at 57 Ma (late Tuerian, Paleocene) with location of study wells (modifield from Strogen 2011).

Mudrock pressure calculations have shown that the Eocene Turi Formation caprock is slightly (∼ 3.5 MPa) overpressured, but the underlying permeable reservoir horizons are close to hydrostatic pressure (Fig. 4). The thin interbedded transgressive marine mudrocks act as vertical pressures seals, producing minor pore-pressure variations between the C-, D-, and F-Sands (Figs. 2, 4, 5).

The F-Sand Depositional Environment

The F-Sands accumulated in a shoreline setting that was oriented NE–SW across the central part of the Taranaki Basin. The F-Sands show a transition from a coastal-plain environment in Maui-1 in the south, to upper and lower-shoreface environments in Tui-1 to the northwest (Fig. 3) (Pollock et al. 2003; Pollock and Crouch 2005; Strogen 2011; Higgs et al.
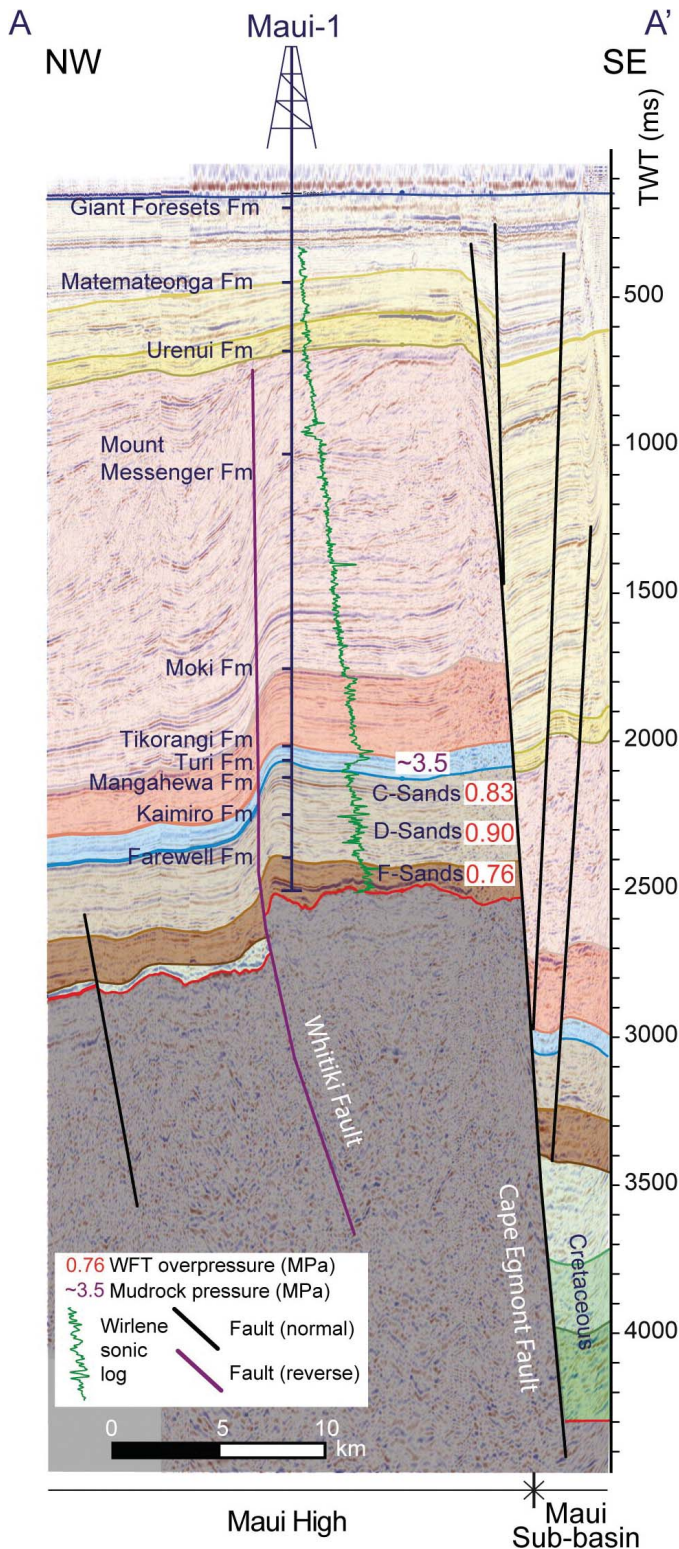
FIG. 4.—Interpreted seismic line through the Maui B Field, displaying Maui-1 well wireline sonic log and associated reservoirs and formation overpressures (calculated using RokDoc). The line of A–A′ section shown in Figure 1 (modified from Line OTS-2, Strogen et al. 2014a).

2012; Strogen et al. 2014b). The F-Sands in Maui-1 displays a low percentage of dinocysts (< 3%) and numerous coal seams, both indicative of a coastal-plain environment (Pollock and Crouch 2005; Higgs et al. 2012; Shiers et al. 2017). The F-Sands in wells MB-R(1) and MB-W(2), drilled to the northeast from the Maui B platform, contain up to 10% glauconite, an authigenic iron potassium phyllosilicate mineral, forming exclusively in marine settings, commonly associated with low-oxygen conditions (Odin and Matter 1981; Odin 1988). Normally, glauconite is considered indicative of shallow marine shelfal environments where the rates of sedimentation are low, but it has been shown to precipitate in dolomitic lagoonal sediments and accumulate in marl–limestone alternations forming in brackish-water estuaries (El Albani et al. 2005). The F-Sands (marginal marine to shoreface facies) and the Farewell Formation (fluvial facies) more generally are thought to have been sourced from erosion of crystalline basement in northwestern South Island and granite-cored structural highs in the Taranaki Basin during the Paleocene (Higgs and King 2018).

Reservoir Stratigraphy.—The F-Sands are 95 mTVD thick in the MB-R(1) well and contain a 30 m oil column (STOS 1993a). Reservoir sandstone beds are interbedded with siltstone beds up to 1.5 m thick, and are often heavily bioturbated. Net-to-gross across all cored intervals is consistently in excess of 90%. The F-Sands are split in the F1 and F0 sands, but both of these intervals are coastal-plain to shoreface deposits in MB-R(1) and MB-W(2) wells (Pollock and Crouch 2005).

METHODOLOGY

Sampling

Cores from the F-Sands in the Maui Field have been cut in two development wells (MB-R(1), 54 m (3218-3263 mTVDss)) and (MB-W(2), 28 m (3232-3252 mTVDss)) from the Maui B Platform (Fig. 1). Sixteen core samples were collected from sandstone beds in both wells from sections that were predominantly clean sandstone without mudrock or coal laminae. Thin sections produced from these samples were observed under transmitted-light microscopy and analyzed by SEM and QEMSCAN (Quantitative Evaluation of Minerals by SCANning electron microscopy). Eleven polished thin sections were provided by Shell Taranaki Ltd. Conventional wireline log data acquired over the cored intervals are representative of the F-Sands across the Maui Field.

Petrographic Analysis.—27 sections were analyzed using transmitted-light microscopy on blue-epoxy-impregnated thin sections, modal analysis (300 counts per section) being undertaken on all samples to ascertain mineralogy. The resulting data were used to calculate intergranular volume (IGV) (Paxton et al. 2002), porosity loss through mechanical compaction (COPL), and porosity loss by cementation (CEPL) (Lundegard 1992):

$$COPL = P_i - \left(\frac{(100 - P_i)P_{mc}}{100 - P_{mc}} \right) \qquad (1)$$

$$CEPL = (P_i - COPL)\left(\frac{C}{P_{mc}} \right) \qquad (2)$$

where P_i is the initial or depositional porosity and P_{mc} is the intergranular volume or minus-cement porosity calculated by subtracting the total cement volume (C) from the total optical primary porosity (P_o). The calculated COPL and CEPL are accurate if three conditions are met. First, the assumed initial porosity (P_i) must be correct. Second, the amount of cement derived by local grain dissolution must be negligible or known. And third, the amount of framework mass exported by grain dissolution must be negligible or known (Lundegard 1992). The initial or depositional porosity of F-Sands has been estimated as 42% (Pryor 1973).
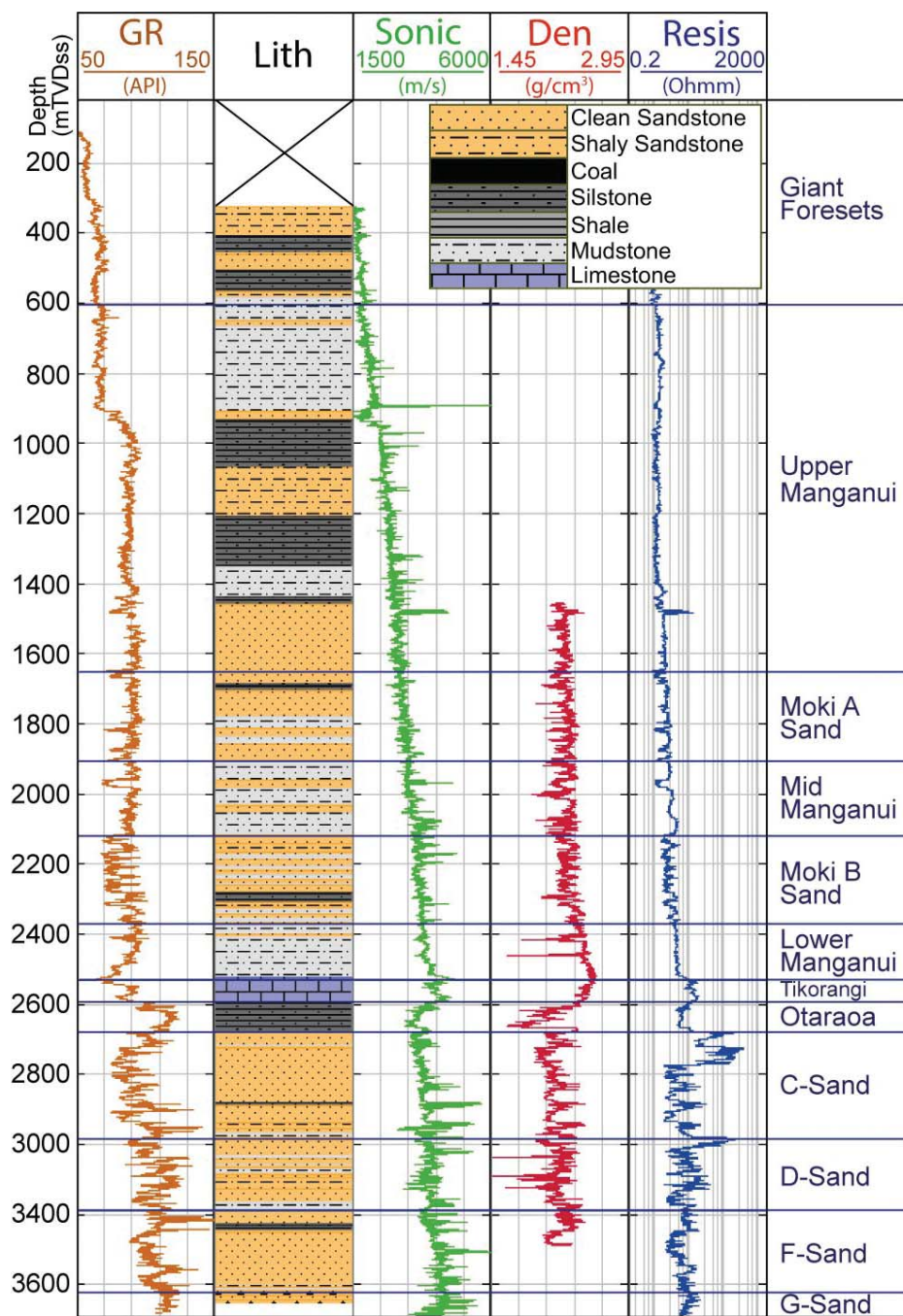
FIG. 5.—Maui-1 wireline log suite and interpreted lithology (gamma ray (brown), sonic velocity (green), density (red), and resistivity (blue)) (SBPT 1969). See Figure 1 for well location. Plotted using RokDoc.

Scanning electron microscopy was undertaken on selected samples, providing additional information on the pore-system geometry, authigenic mineralogy, and paragenetic relationships. All thin sections were highly polished to 30 μm and coated with 30 nm of carbon before analysis by a Hitachi SU-70 field-emission scanning electron microscope (SEM) equipped with an energy-dispersive detector (EDS). Backscatter scanning electron microscopy of thin sections was conducted at acceleration voltages of 15 kV with a beam current of 0.6 nA. The SEM-EDS assembly was used for rapid identification of chemical species and their orientation in the sample. The analysis was undertaken on gold palladium coated, freshly broken samples glued onto aluminum stubs with silver paint.

QEMSCAN data were collected (20 μm spacing) from polished and carbon-coated thin sections at three representative sample depths, two medium to coarse-grained sandstones (3229.16 TVDss (MB-R-(1)); and 3238.7 TVDss (MB-W(2)) and one very fine-grained sandstone (3232.33 TVDss (MB-W(2)), in order to supplement scanning electron microscopy and modal analysis. QEMSCAN analysis measures and identifies minerals within a defined sample area, using a scanning electron microscope (SEM) fitted with four light-element X-ray energy-dispersive spectrometer detectors, allowing for fast, quantitative, and repeatable mineralogical and rock texture analyses (e.g., Higgs et al. 2015).

One-Dimensional Burial History Modeling

The evolution of formation temperature in the stratigraphy intersected by MB-R(1) in the Maui Field was modeled in one dimension using

Schlumberger's *PetroMod*™ (V. 2015) software. PetroMod is based on a forward-modeling approach to calculate the geological evolution of a basin from its burial history (Hantschel and Kaueraauf 2009). The burial model uses well stratigraphy and associated lithologies from mud-log cuttings data recorded in the well-completion report (STOS 1993a). The lithological units used are mainly PetroMod (V. 2015) default lithologies, which have been mixed based on well-log descriptions, mud log cuttings, and core analysis reports for the wellbore.

The model was calibrated against corrected bottom-hole data for the Maui Field (Rob Funnell, personal communication 2018), fluid-inclusion microthermometry (Killops et al. 2009), and helium-porosity data (Fig. 6A, B) (STOS 1993a, 1993b). The law for porosity loss with depth was used, because it utilizes effective stress rather than total depth and is applicable for a wide range of rock types (Hantschel and Kaueraauf 2009). Heat flow was estimated after Funnell et al. (1996), uplift from Armstrong et al. (1998), and paleo-water depths were extracted from biostratigraphy in the well completion report (STOS 1993a).

RESULTS

F-Sand Sandstone Composition

The F-Sands in the Maui Field can be characterized as arkosic arenites (Fig. 6A) with abundant quartz (Q: 36–60%, av. 46%) and feldspar (Fspr: 14–35%, av. 24%); lithic rock fragments of granite, schist, arenite, and volcanics make up an av. 4% of the grains (Fig. 6A, Table 1). The sandstones are moderately sorted, medium to coarse-grained, and mineralogically moderately mature (Fig. 7A, B). The detrital grains range in size from very fine to very coarse sand and are predominantly subangular to subrounded (STOS 1993b, 1993a) (Fig. 7A, B, 8A). Both orthoclase and plagioclase feldspars are present and display various stages of alteration from fresh to highly corroded (Figs. 7A, 8A, 9A) and rarely display overgrowths. QEMSCAN analyses record up to 40% feldspar content (av. 23% plagioclase and av. 13% orthoclase; Table 2). Very rare preserved skeletal carbonate grains are present in one-third of the samples. Rare, primary pore-filling authigenic clay minerals form between 0 and 10% of the sandstone (Fig. 9F; Table 1). Detrital micas are present in most sections, varying between 0 and 3% in abundance (Table 1), with high percentages occurring in sandstones with interbedded mudrock beds. Micas can vary between being undeformed to heavily deformed, both broken and bent (e.g., Fig. 8E). Detrital mud clasts can form up to 6% of the rock volume (Table 1). QEMSCAN (Fig. 7A, B) analyses identified the presence of titanium oxide (1–3%). Hydrocarbon streaks are present in primary intragranular porosity and very rarely fracture porosity (Fig. 8C). Grains of yellow to bright green glauconite are present (0.7–10.7%) in every sample (Fig. 8A, B), many of which are deformed and degraded (Fig. 7A, B).

Mechanical Compaction.—Maui Field F-Sand samples display mechanical compaction of soft grains, such as deformed lithic clay grains, kinked mica grains, and chemical compaction features such as concavo-convex grain contacts at boundaries of detrital quartz grains (Fig. 8A). Mechanical compaction led to fracturing of both feldspar and quartz grains and bending and breaking of micas (Fig. 8E). The average values for porosity loss due to compaction (28%) and cementation (5%) from Figure 6E (Lundegard 1992) show that mechanical compaction, rather than cementation, is the main driver of porosity loss in the Maui F-Sands.

Authigenic Clay Minerals.—Authigenic clay minerals are not common in any of the thin sections under transmitted light, rarely filling pore space (Fig. 9F) and never rimming whole grains. SEM, SEM-EDS, and QEMSCAN analyses identified sporadic thin chlorite grain-coating alongside mixed-layer illite–smectite coats, which are in places impeding

the nucleation and growth of quartz overgrowths (Fig. 9D). Kaolinite booklets can, on rare occasions, fill intergranular porosity and also bridge pore throats (Fig. 9F). Heavily degraded glauconite grains, observed in both reflected light, SEM, and QEMSCAN, show progressive alteration to kaolinite and chlorite (Figs. 7, 9B).

Carbonate Cement.—Carbonate cements are localized throughout the F-Sands occurring as isolated patches typically composed of euhedral sparitic calcite cement fills (Fig. 9E) and partially or fully replacive of detrital grains (Fig. 7A). Calcite cement can also be found between cleavage planes of mica grains (Fig. 8F). QEMSCAN analyses (Fig. 7A) support the hypothesis that calcite cement is sporadically developed in the samples and host rocks and that it occludes secondary porosity. Modal analysis from all thin sections has shown calcite to contribute up to 5% of the rock volume.

Quartz Cementation and Fluid Inclusions.—Minor pressure dissolution of quartz grains has been identified in reflected-light microscopy (Fig. 8A) and in backscatter SEM images (Fig. 10A). Quartz cements are recognized in all samples used in this study, dominated by blocky and sometimes thick macro-quartz overgrowths present on generally non-coated detrital-quartz grain surfaces (Fig. 10A). The macro-quartz overgrowths are defined as syntaxial quartz overgrowth larger than 20 μm in optical continuity with the host detrital quartz grain. They are euhedral and contain abundant fluid inclusions in dust rims and pitted crests (Fig. 9C). Although quartz cement is common amongst the samples in this study, it usually contributes only 2% of the bulk rock and up to 6% in some (Table 1). The formation of quartz overgrowths may have been inhibited by the presence of chlorite coating on grains (Fig. 9D). Killops et al. (2009) identified appreciably more aqueous inclusions than oil inclusions in quartz overgrowths from the F-Sands in the Maui Field. Oil inclusions occurring in dust rims between grains and overgrowths document multiple phases of hydrocarbon charge. Homogenization temperatures of quartz aqueous inclusions are between 93°C to 127°C (Killops et al. 2009).

Porosity.—Results of core analysis (Fig. 6B) show that helium reservoir porosities range between 3 and 22% (av. 16.2%) (STOS 1993a, 1993b). Total porosity is a combination of primary intergranular (11.4%; Table 1, Figs. 6C, 8B), secondary dissolution (av. 1.7%; Table 1, Fig. 8A), hydrocarbons (0.8%; Table 1, Fig. 8C), very minor fracture porosity, and microporosity. Visible primary intergranular and secondary dissolution pores are often interconnected, aided through minor fracturing of feldspar grains. Secondary pores are formed through corrosion of feldspars, producing honeycomb textures (STOS 1993a) (Figs. 8A, 9A). The final present-day basin-modeling-derived porosity of ∼ 18% (Fig. 6F) matches the average helium porosity when fine-grained intervals are excluded. Rare grain-size pores are evidence for total dissolution (Fig. 8A), though there is a possibility that some of these are artefacts of sample preparation. The limited amount of authigenic pore-filling or pore-throat blocking clay cement types (av. 3%) would have assisted in maintaining high permeability (av. 419 mD; Fig. 6B).

Burial History Modeling

Deposition of the F-Sands began during the early Paleocene (Fig. 11) in a shoreface to inner-shelf setting (Strogen 2011), as indicated by the high net-to-gross, presence of glauconite, and poorly developed thin shale horizons. These deposits experienced slow initial subsidence rates of 32 m/My. During the early Oligocene the basin was starved of sediment and subsidence rapidly increased (King and Thrasher 1996; Strogen et al. 2014b), resulting in bathyal water depths (Fig. 11). Sedimentation rates increased to 330 m/My during the late early Miocene due to the

TABLE 1.—*Model point-count summary (300 counts) for the F-Sands at the Maui Field (IGV, intergranular volume; COPL, porosity loss due to mechanical compaction; CEPL, porosity loss due to chemical compaction). Thin sections provided by Shell Taranaki denoted using an asterisk after the well name e.g. MB-R(1)*. x in cells denotes samples/sections used for SEM, BSEM, and QEMSCAN analyses.*

Well	Depth [m] MDAH	Depth [m] TVDss	Quartz [%]	Lithics [%]	Feldspar [%]	Carbonate Grain [%]	Intergranular Carbonate Cement [%]	Carbonate replacement cement [%]	Heavy Mineral [%]	Mud Clast [%]	Hydrocarbon [%]
MB-R(1)*	3516.38	3218.90	54.3	5.3	17.3		0.3		1.0	0.3	0.3
MB-R(1)	3516.40	3218.95	60.0	3.3	12.0		1.3	0.3	1.0	0.7	
MB-R(1)*	3517.93	3218.92	50.0	3.7	18.7			0.0	1.0	1.0	
MB-R(1)	3518.30	3219.40	45.0	6.0	13.7		0.3		1.7	1.3	0.7
MB-R(1)*	3520.91	3221.62	48.0	2.3	27.0	0.3			0.7	4.3	0.7
MB-R(1)	3525.50	3225.88	43.3	4.0	27.3		0.3		0.3	0.3	0.3
MB-R(1)	3529.20	3229.16	50.7	5.3	21.3	0.3		0.3	0.3		
MB-R(1)*	3531.94	3231.60	48.0	4.3	23.7		0.3		0.3	0.3	
MB-R(1)	3535.20	3234.57	53.0	4.7	20.0	0.3	0.3	0.3		0.3	1.0
MB-R(1)	3539.20	3238.07	54.3	4.7	20.3	0.7			0.7	0.3	
MB-R(1)	3545.20	3243.47	50.7	4.7	23.0	0.3	0.3	1.3	0.7	0.3	
MB-R(1)*	3548.41	3246.17	51.7	3.0	19.3		1.7		0.3	1.7	1.0
MB-R(1)	3560.90	3257.82	50.3	2.0	25.0	0.3	3.0	1.7	1.0		
MB-R(1)	3565.25	3261.69	44.0	8.3	23.3		2.0		0.3		0.3
MB-R(1)	3569.90	3262.77	52.0	5.0	19.0		1.0	0.3			0.7
MB-W(2)	4111.20	3232.33	40.3	2.3	22.3		3.0	1.3	0.3	0.3	0.7
MB-W(2)*	4113.88	3234.71	35.7	4.3	30.0				0.7	0.3	0.3
MB-W(2)	4115.20	3235.89	40.3	3.0	29.3		3.0	0.3	0.3	1.3	0.7
MB-W(2)*	4118.30	3238.65	42.0	1.0	35.0					1.3	
MB-W(2)*	4120.10	3240.26	48.3	1.0	30.0		0.7		0.3	0.7	0.7
MB-W(2)	4121.10	3241.15	41.3	3.0	31.0	0.3	0.3		1.3	1.0	
MB-W(2)*	4124.88	3244.53	44.3	4.7	22.7				0.3	2.0	1.0
MB-W(2)	4125.30	3244.91	44.0	6.7	24.7		1.3		0.3	0.3	
MB-W(2)	4126.20	3245.71	42.3	4.3	24.0		0.7		0.7	1.0	0.7
MB-W(2)*	4127.60	3246.96	40.7	2.7	31.7	0.3	1.0	0.3		0.3	0.3
MB-W(2)*	4129.40	3248.58	42.3	2.7	24.0				0.7	5.7	3.3
MB-W(2)	4133.20	3251.98	40.7	4.7	30.7	0.3	0.3			0.3	0.3

progradation of Moki Formation basin-floor fans and associated mudrocks of the Manganui Formation (Fig. 11). By the late Miocene ($\sim$ 6 Ma) the rate of burial, particularly in southern and central parts of the Taranaki Basin, would have slowed and anticlinal inversion structures formed together with widespread uplift of the southern Taranaki Basin (Kamp and Green 1990; Crowhurst et al. 2002; Bull et al. 2019).

The structural development of the Maui trap occurred during this period, at $\sim$ 8–6 Ma (King and Thrasher 1996; Funnell et al. 2004; Reilly et al. 2016), which coincided with the initial hydrocarbon charge into the Maui Field (Killops et al. 2009). The trapping temperature (av. 103°C) inferred from the homogenization of aqueous inclusions was reached at 7–7.5 Ma (Killops et al. 2009), towards the end of the deposition of the Manganui Formation. The burial history (Fig. 11) shows that trapping occurred close to maximum burial depth. Rates of subsidence reduced during the Pliocene due to a further reactivation of the Cape Egmont Fault, resulting in footwall (location of the Maui Field) uplift which almost overcame reginal subsidence (Reilly et al. 2016).

Diagenetic Paragenesis

Mechanical compaction (porosity loss) of the F-Sands in the Maui Field began during shallow burial from $\sim$ 50 Ma (Figs. 12, 13). Continued increases in vertical effective stress due to burial led to deformation of labile grains (micas and glauconite) and later formation of concavo-convex and long grain contacts. The minor grain fracturing observed will have formed throughout burial due to pressure at grain point contacts (Chuhan et al. 2002, 2003) and potentially during uplift of the Maui structure (e.g.,

Reilly et al. 2016). Carbonate cementation may have started at shallow depths, demonstrated by the occurrence of initial pore-filling calcite cement, supported by the lack of grain–grain point contacts in some thin sections, and has been identified elsewhere in the Paleocene of the Taranaki Basin (e.g., Martin et al. 1994; O'Neill et al. 2018).

The onset of feldspar and mica degradation may have occurred during shallow burial, contemporaneous with the precipitation of kaolinite (Bjorlykke 1998; Lanson et al. 2002) (Fig. 12). Detrital glauconite grains have been observed to be heavily deformed and would have begun to dissolve approaching maximum burial depth and associated temperatures above 100–110°C (Hansley and Nuccio 1992; Ivanovskaya et al. 2003). Iron released during the degradation of glauconite has been shown in other basins to reprecipitate as chlorite (Hansley and Nuccio 1992; Shannon Sandstone, Wyoming). This process could account for chlorite rims observed on detrital grains in the F-Sands. Fluid-inclusion data collected by Killops et al. (2009) established that quartz cementation started at approximately 93°C in the F-Sands in the Maui Field, with a main phase occurring between 97°C and 107°C. In-situ temperature inferred by homogenization of aqueous inclusions was reached at 7.0–7.5 Ma, towards the end of accumulation of the Manganui Formation (Fig. 11; Killops et al. 2009). The liberation of silica from feldspar degradation and subsequent clay reactions aided in the nucleation and growth of quartz overgrowths (Fig. 12; e.g., Worden and Morad 2009).

Oil charging is interpreted to have begun at $\sim$ 6 Ma (King and Thrasher 1996; Funnell et al. 2004) associated with the flushing of aggressive acidic fluids, which has also been demonstrated in the Kapuni Field (Higgs et al. 2013; O'Neill et al. 2018). This acidic flushing may have led to enhanced

TABLE 1.—*Extended.*

Well	Mica [%]	Clay Cement [%]	Quartz Overgrowth [%]	Intergranular Porosity [%]	Secondary Porosity [%]	Glauconite [%]	Feldspar Overgrowth [%]	IGV [%]	COPL [%]	CEPL [%]	SEM	BSEM	QEMSCAN
MB-R(1)*			2.7	12.3	5.3	0.7		15.7	31.2	2.1			
MB-R(1)	3.0	2.3	1.0	12.0	1.7	1.3		17.0	30.1	3.5			
MB-R(1)*	1.7	2.0	4.3	9.7	4.7	3.0	0.3	16.3	30.7	4.6			
MB-R(1)	1.3	4.0	6.3	13.0	2.0	2.3	2.3	26.7	20.9	10.3			
MB-R(1)*	0.7	5.0	1.7	4.3	4.3	0.3	0.3	12.0	34.1	4.6	x		
MB-R(1)	2.0	2.7	2.7	10.3	3.0	3.0	0.3	16.7	30.4	4.2			
MB-R(1)	0.3	2.0	3.0	11.7	2.0	2.0	0.7	17.7	29.6	4.2			x
MB-R(1)*	1.3	0.3	2.0	12.7	3.3	2.7	0.7	16.0	31.0	2.3			
MB-R(1)	0.7	2.0	1.3	11.0	0.7	4.0	0.3	16.3	30.7	3.0			
MB-R(1)		2.0	2.3	12.0	1.3	0.7	0.7	17.0	30.1	3.5		x	
MB-R(1)	0.3	0.3	2.3	11.3	1.0	2.7	0.7	16.3	30.7	3.5			
MB-R(1)*	1.3		1.0	13.0	1.7	4.0	0.3	17.0	30.1	2.1			
MB-R(1)		1.7	2.0	10.7		1.7	0.7	19.7	27.8	6.5			
MB-R(1)		2.3	1.0	15.7	0.3	2.3	0.0	21.3	26.3	3.9	x		
MB-R(1)	0.7	6.3	0.7	12.7	0.3	1.0	0.3	22.0	25.6	6.4			
MB-W(2)	5.0	10.0	0.3	3.3		10.7		18.7	28.7	10.5			x
MB-W(2)*	1.0	8.7	1.7	9.3	1.3	6.7		20.0	27.5	7.5			
MB-W(2)	1.0	1.7	0.7	13.3		4.7	0.3	20.0	27.5	4.4			
MB-W(2)*	1.0	2.3	3.0	9.3	0.7	3.7	0.7	15.3	31.5	4.1			x
MB-W(2)*	0.7		1.3	13.3	1.0	1.7	0.3	16.3	30.7	1.6			
MB-W(2)	1.0	2.0	2.0	13.0	0.3	2.7	0.7	18.0	29.3	3.5		x	
MB-W(2)*	1.0	6.3	3.3	4.3	1.7	7.7	0.7	15.7	31.2	7.1			
MB-W(2)	0.3	1.0	3.0	14.3	0.3	3.0	0.7	20.3	27.2	4.4	x		
MB-W(2)	0.7	4.3	1.3	15.0	0.3	3.3	1.3	23.3	24.3	5.8			
MB-W(2)*		1.0	2.0	15.7		3.3	0.7	21.0	26.6	3.7			
MB-W(2)*	1.3	2.0	2.3	10.7	1.0	3.3	0.7	19.0	28.4	3.6		x	
MB-W(2)	0.3	2.7	2.3	14.7		1.7	1.0	21.3	26.3	4.7			

dissolution of carbonate cement and of framework grains and etching of quartz overgrowths. Late-stage carbonate cementation is also still occurring, as shown by precipitation into secondary porosity (Fig. 13).

DISCUSSION

The locally excellent reservoir quality of the F-Sands reservoir in the Maui Field is mainly due to three key factors: the relatively shallow depth of burial, limited amount of both authigenic silica and clay cements, and the formation and preservation of secondary porosity (Fig. 13). The F-Sands could be characterized as a geochemically closed system, where dissolved solutes are redistributed within the reservoir section.

Reservoir Quality

Although some primary intergranular porosity has been lost through mechanical compaction, the effective stress conditions of the reservoir are still relatively low (33.1 MPa). The onset of silica cementation can occur in the range between 70 and 100°C (Bjørlykke and Egeberg 1993), but the start of significant silica cementation typically occurs between 90 and 100°C (Giles et al. 2009). Basin modeling results suggest that the F-Sands have experienced a maximum temperature of 105°C (Fig. 11), suggesting that silica cement could be significant, but this is not the case. The limited occurrence of quartz cement in the F-Sands could be due their late entrance into the chemical-compaction window (> 2500 m) only some 10 My ago and with only ~ 7 My residence in the realm of significant quartz cementation. Chlorite grain coatings have been shown, in places, to limit the nucleation and growth of quartz overgrowths (Fig. 9D; e.g., Ehrenberg 1993; Stricker and Jones 2016; Stricker et al. 2016).

The limited volume of both pore-filling clay and quartz cement has left pore throats open, resulting in excellent permeability and thus connectivity within the reservoir (Fig. 8B). This has been enhanced through formation of secondary dissolution porosity (Figs. 8A, 9A) and some minor fracturing (Chuhan et al. 2002; Reilly et al. 2016). Additionally, the limited ductile-grain content combined with the moderately well sorted nature of the sandstones, led to moderate-efficiency grain packing, helping to prevent porosity loss via compaction (Paxton et al. 2002). This is suggestive of a facies control on reservoir quality, as demonstrated in many other reservoirs in shelfal to shoreface facies (e.g., Mansurbeg et al. 2008; Ambrose et al. 2017; Haile et al. 2018; Porter et al. 2018). Conversely, the ductile nature of glauconite grains (Ranganathan and Tye 1986) would have enabled non-elastic deformation of the sandstones (Hossain et al. 2009), which directly affects reservoir quality by potentially blocking pore throats, but the relatively low glauconite content means that this would only be a secondary process.

The present-day reservoir quality of the Farewell Formation in Maui Field is a cumulative product of depositional attributes (facies and grain size), mechanical compaction, and diagenesis during early and late stages of burial (Figs. 11, 12, 13). Mechanical compaction and late generation of secondary porosity are also the most significant diagenetic processes which would have occurred in Farewell Formation at Kapuni Deep-1 (O'Neill et al. 2018), which is the deepest well (> 5500 m) that sampled the Paleocene in the Taranaki Basin. The COPL-CEPL analyses, minor grain fracturing, and grain deformation, all suggest that mechanical compaction
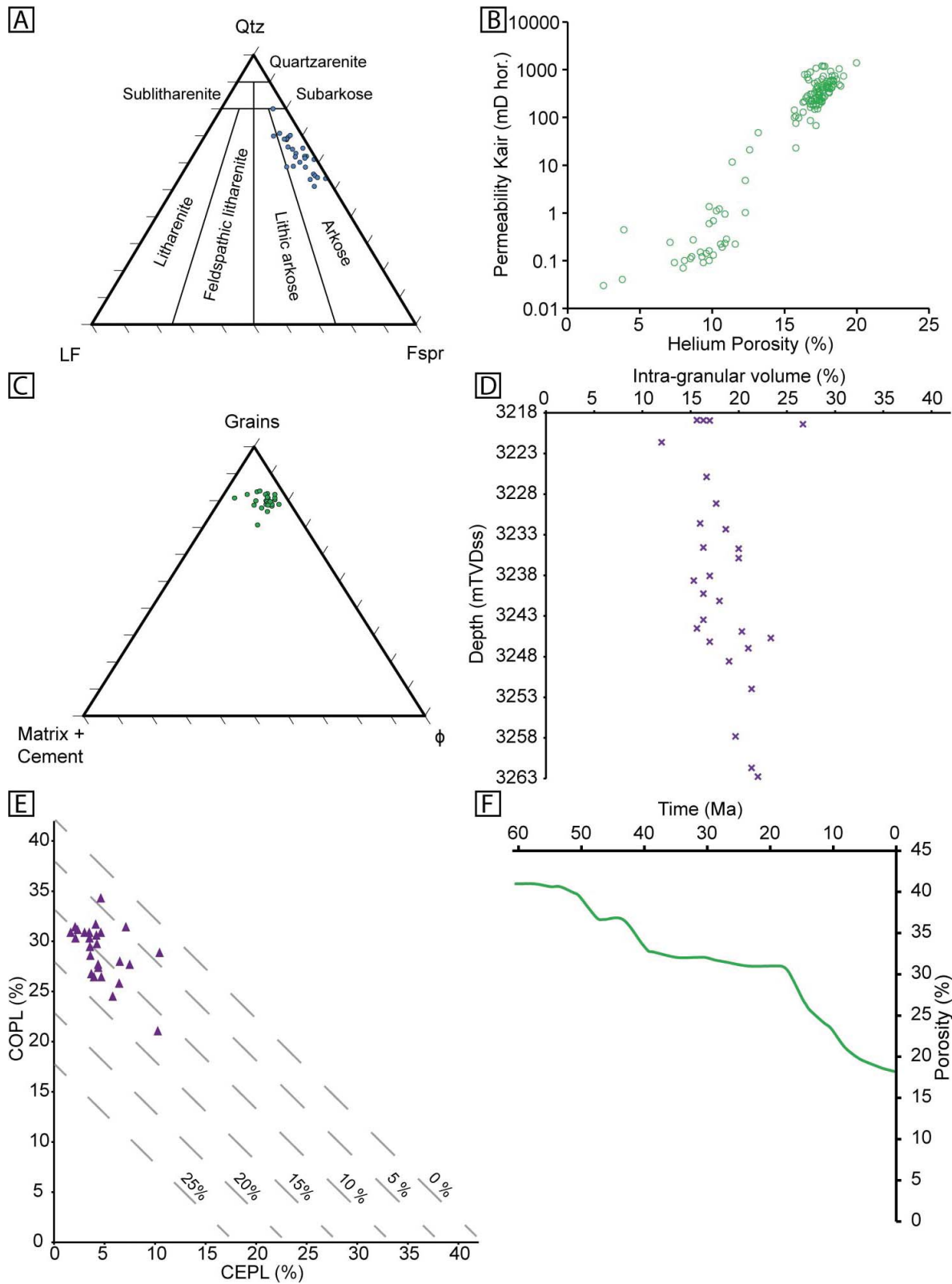
FIG. 6.—**A)** Ternary plot of present-day composition of the F-Sands at MB-R(1) and MB-W(2) from modal point-count data (Table 1). **B)** Measured porosity permeability cross-plot from core-analysis data of the F-Sands at MB-R(1) and MB-W(2) (STOS 1993a, 1993b). **C)** Ternary plot displaying grain:matrix:porosity ratio of F-Sands at MB-R(1) and MB-W(2) from modal point-count measurements. **D)** Plot of intergranular volume against depth in the F-Sands at MB-R(1) and MB-W(2). **E)** Compactional (COPL) and cementational (CEPL) porosity loss for the F-Sands at MB-R(1) and MB-W(2) with remaining sample porosity (dashed lines). COPL and CEPL is calculated after Lundegard (1992). **F)** Plot of modeled porosity development of F-Sands at MB-R(1) well against time, from 1D basin modeling (Fig. 11).

| Background (φ) | | Plagioclase | | Smectite | | Kaolinite | | Ti oxide | | Illite-Fe/ |
| Quartz | | Orthoclase | | Illite | | Chlorite | | Calcite | | Glauconite |
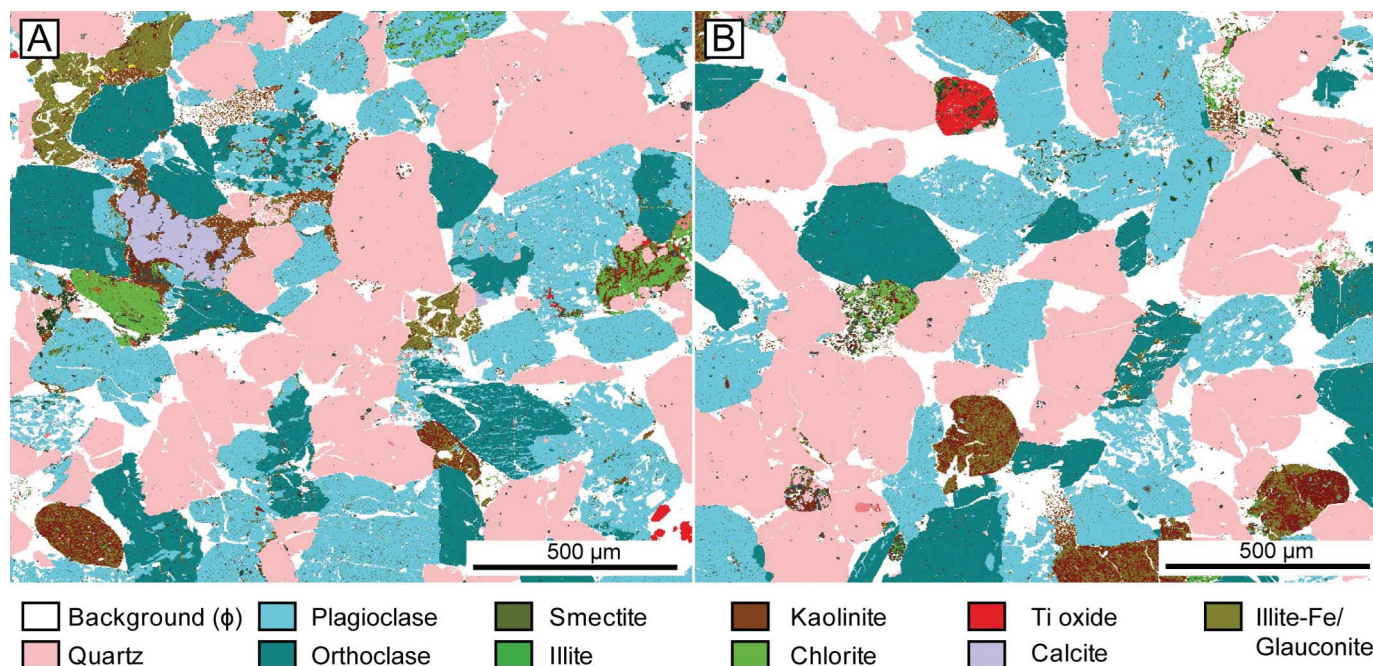
Fig. 7.—QEMSCAN images of the F-Sands in the Maui Field (2 μm point spacing). **A)** Degraded feldspar grains, heavy-mineral, fractured quartz grains, and connected intergranular porosity (3238.65 TVDss; MB-W(2)). **B)** Calcite cement filling secondary porosity, degraded orthoclase and glauconite grains, minor pore-filling kaolinite, and pressure solution contacts (3238.65 TVDss; MB-W(2)).

was the key driving mechanism for porosity reduction during the first 2500 m of burial through the steady increase of vertical effect stress.

CO₂ and Secondary Porosity

CO_2-rich fluids have been shown to contribute towards feldspar dissolution in clastic reservoirs (Lundegard and Land 1986; Hansley and Nuccio 1992; Higgs et al. 2013; Cao et al. 2014; Yuan et al. 2015b). Experimental work (e.g., Wang et al. 2017) and numerical modeling (e.g.,

TABLE 2.—Summary of QEMSCAN data (20 μm pixel spacing) for two medium- to coarse-grained sandstones (3229.16 TVDss (MB-R-(1)); and 3238.7 TVDss (MB-W(2)) and one fine- to very fine-grained sandstone (3232.33 TVDss (MB-W(2)) from the F-Sands of the Maui Field.

Depth (mTVDss)	3529.2	4119.3	3232.33
Well Name	MB-R(1)	MB-V(2)	MB-R(1)
Background (φ)	21.39	25.64	1.88
Quartz	34.55	28.43	31.02
Plagioclase	23.81	24.37	22.07
K-Feldspar	16.77	13.86	8.34
Calcite	0.05	0.14	0.04
Illite	0.06	0.09	0.41
Illite-Fe/Glauconite	0.43	1.96	6.28
Smectite	0.72	0.78	1.81
Chlorite	0.72	0.51	12.50
Kaolinite		0.77	0.45
Muscovite	0.17	0.30	0.56
Biotite	0.50	1.88	7.90
Pyrite	0.02	0.09	0.46
Rutile	0.18	0.24	0.47
Apatite	0.02	0.07	0.33
Others	0.05	0.01	0.05
Salts/"salt muds"	0.01	0.19	
Unclassified	0.53	0.65	5.23

Barclay and Worden 2000; Xu et al. 2005) further supports the dissolution of feldspar by CO_2-rich fluids. The flow of acidic CO_2-rich fluids is an important mechanism particularly driving dissolution of carbonate cements and detrital grains and generating secondary porosity in the Kapuni Field, Taranaki Basin (Higgs et al. 2013; O'Neill et al. 2018), and producing oversized pores in some Taranaki reservoirs (Collen and Newman 1991). Dissolved CO_2 in pore fluids in the F-Sands could also have driven feldspar dissolution, producing honeycomb-texture secondary porosity as noted above.

The Maui Field oil has been typed to a Late Cretaceous coaly source with a marine contribution (mostly likely the Rakopi Formation; Fig. 2) (Sykes et al. 2012), which is also potentially providing associated CO_2 through thermal decarboxylation of the coal beds. The source location is more enigmatic, but it has been suggested that the most likely area is the adjacent Maui Sub-basin, and migration is facilitated through the Cape Egmont Fault, which bounds the field to the east (Funnell et al. 2001; Reilly et al. 2016). Coaly source rocks present in the Paleocene stratigraphy of the Maui structure are immature for CO_2, but modeling of the adjacent Maui Sub-basin suggests that the Rapoki Formation is mature for CO_2 expulsions (Funnell et al. 2001). Microthermometry carried out by Funnell et al. (2001) of fluid inclusions from the overlying C- and D-Sands in the Maui Field suggest an initial charge of hot brines (150°C) with high CO_2 content, at ~ 10 Ma. High trapping temperatures, when compared to maximum reservoir temperatures in the F-Sand, is suggestive of advective fault-controlled flow up the Cape Egmont Fault (Funnell et al. 2001), and the potential charging of the F-Sands.

A second minor charge of high CO_2 brines (135°C trapping temperature) associated with an initial oil influx, occurred at ~ 5 Ma (Funnell et al. 2001), when reverse displacement on the Cape Egmont fault juxtaposed Cretaceous and Paleocene reservoirs, facilitating the cross-fault flow of hydrocarbons and CO_2 (Reilly et al. 2016). The suggested relatively short migration pathway of these acidic fluids would restrict them from reaching equilibrium with pore waters, leading to etching and degradation of detrital grains in the F-Sands of the Maui Field. Bitumen-filled pore
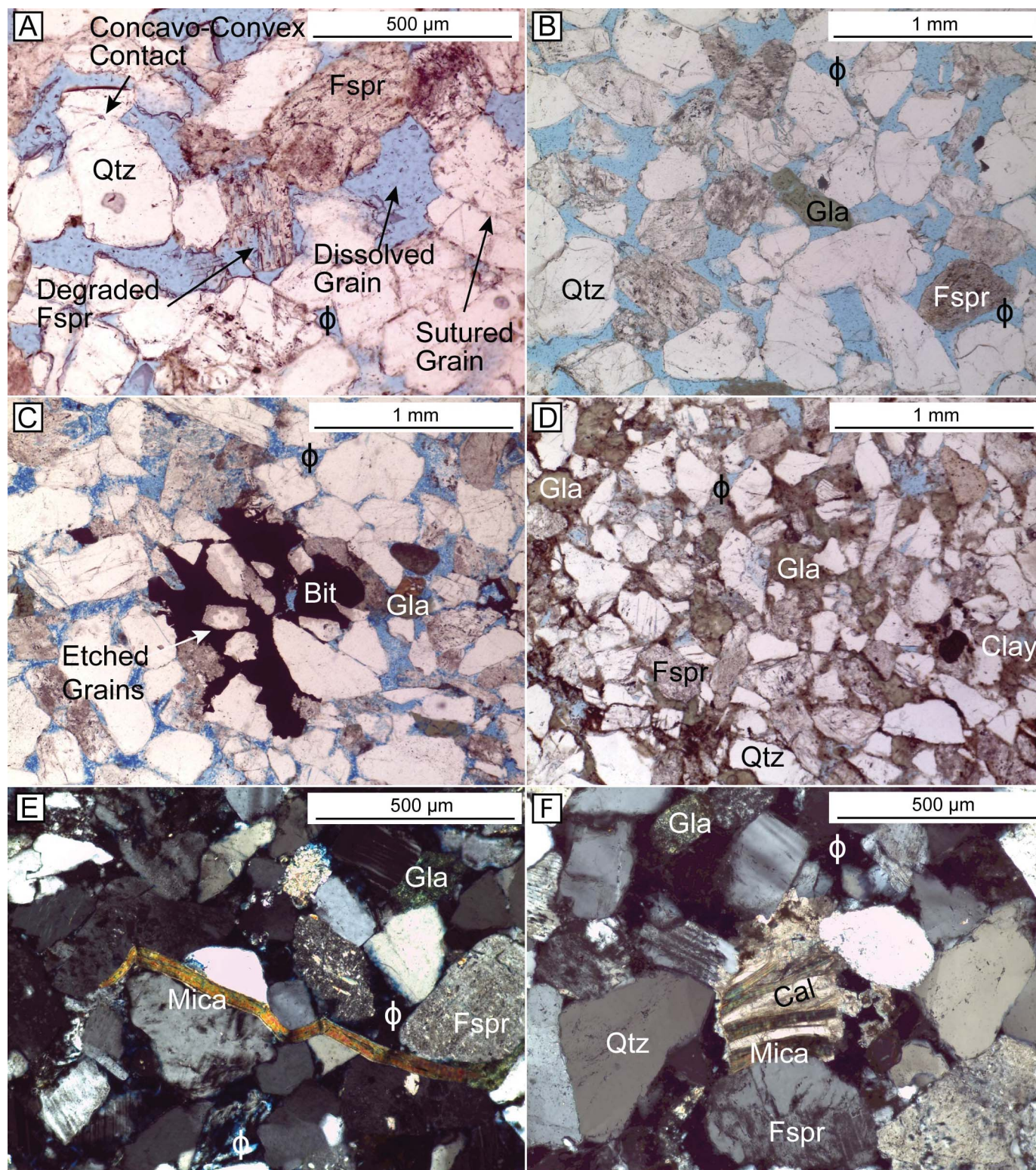
FIG. 8.—Thin-section micrographs of the F-Sands in the Maui Field. **A)** Medium to coarse-grained sandstone with concavo-convex contacts, sutured grain contacts, dissolved grains, and degraded feldspars (PPL; 3219.0 mTVDss; MB-R(1)). **B)** Medium to coarse-grained sandstone with connected intergranular porosity and glauconite (PPL; 3251.82 mTVDss; MB-R(1)). **C)** Medium-grained sandstone with bitumen-filled pore space and associated etched grain rims (PPL; 3240.20 mTVDss; MB-W(2)). **D)** Fine to very-grained sandstone displaying abundant glauconite and clay cement, and limited visible intergranular porosity (PPL; 3232.33 mTVDss; MB-W(2)). **E)** Medium to coarse-grained sandstone with deformed mica and glauconite grain (XPL; 3238.70 mTVDss; MB-W(2)). **F)** Medium to coarse-grained sandstone with calcite cement growing between cleavage planes in a mica grain (XPL; 3244.90 mTVDss; MB-W(2)). (Fspr, feldspar; Qtz, quartz; Gla, glauconite; ϕ, porosity; Bt, bitumen; cal, calcite cement).
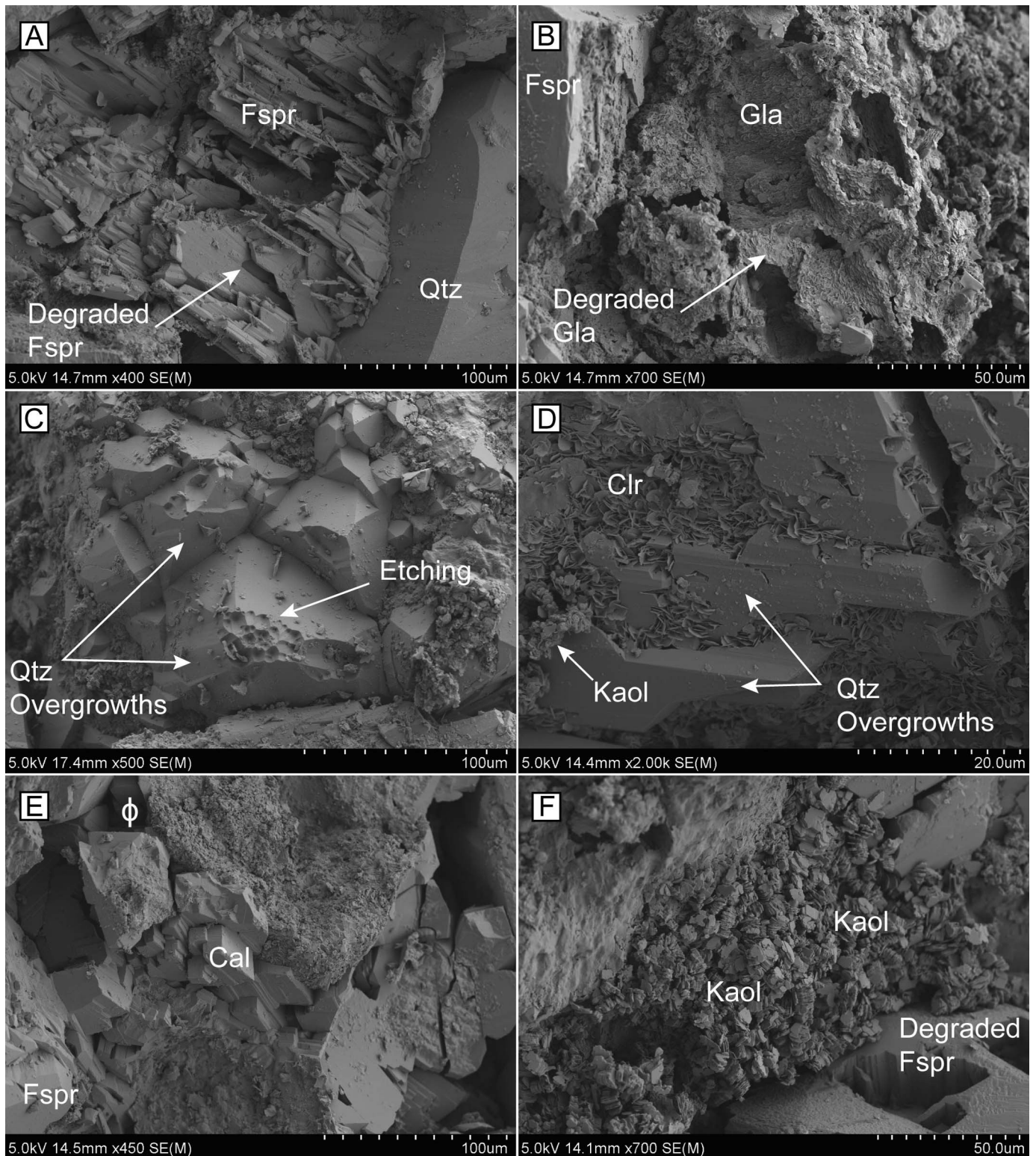
FIG. 9.—SEM images of the F-Sands in the Maui Field. **A)** Heavily degraded feldspar grain displaying honeycomb porosity (3244.91 mTVDss; MB-W(2)). **B)** Heavily degraded glauconite grain (3261.69 mTVDss; MB-R(1)). **C)** Macro-quartz overgrowths with etched crests (3244.91 mTVDss; MB-W(2)). **D)** Quartz overgrowths and grain-coating chlorite (3261.69 mTVDss; MB-R(1)). **E)** Pore-filling calcite cement and open inter-granular porosity (3244.91 mTVDss; MB-W(2)). **F)** Degraded feldspar and pore-filling kaolinite (3244.91 mTVDss; MB-W(2)). (Fspr, feldspar; Qtz, quartz; Gla, glauconite; φ, porosity; Clr, chlorite; Kaol, kaolinite; Cal, calcite cement).
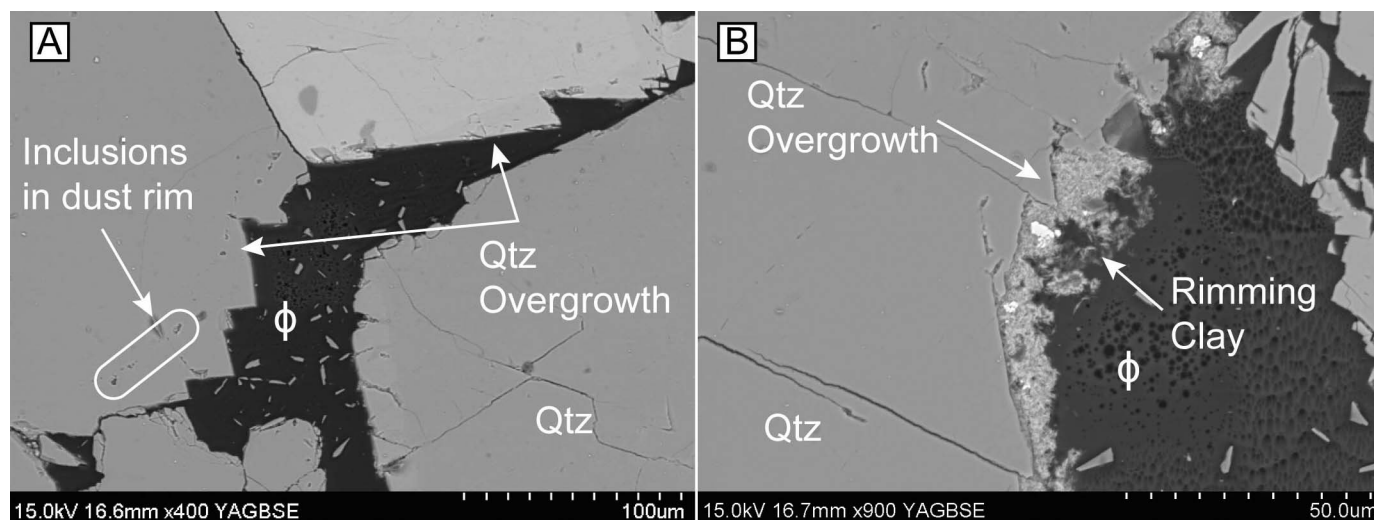
FIG. 10.—BSEM images of the F-Sands in the Maui Field. **A)** Fluid inclusions trapped in the dust rim of macro-quartz overgrowths (3238.07 mTVDss; MB-R(1)). **B)** Mixed clay coating on surface of quartz overgrowth (3248.58 mTVDss; MB-W(2)). (Qtz, quartz; φ, porosity)

space surrounded by etched grains (Fig. 8C) and pitted crests of quartz overgrowths (Fig. 9C) identified in the F-Sands is suggestive of aggressive acidic fluids, which could enhance secondary porosity. The relatively recent charging of acidic fluids approaching maximum burial, and associated dissolution, would have weakened the grain framework, but

limited subsequent burial has reduced the potential for secondary compaction, which has helped contribute to the preservation of secondary porosity in the F-Sands.

Furthermore, dissolution of detrital grains in sandstones is frequently postulated to occur in the presence of low-salinity meteorically sourced
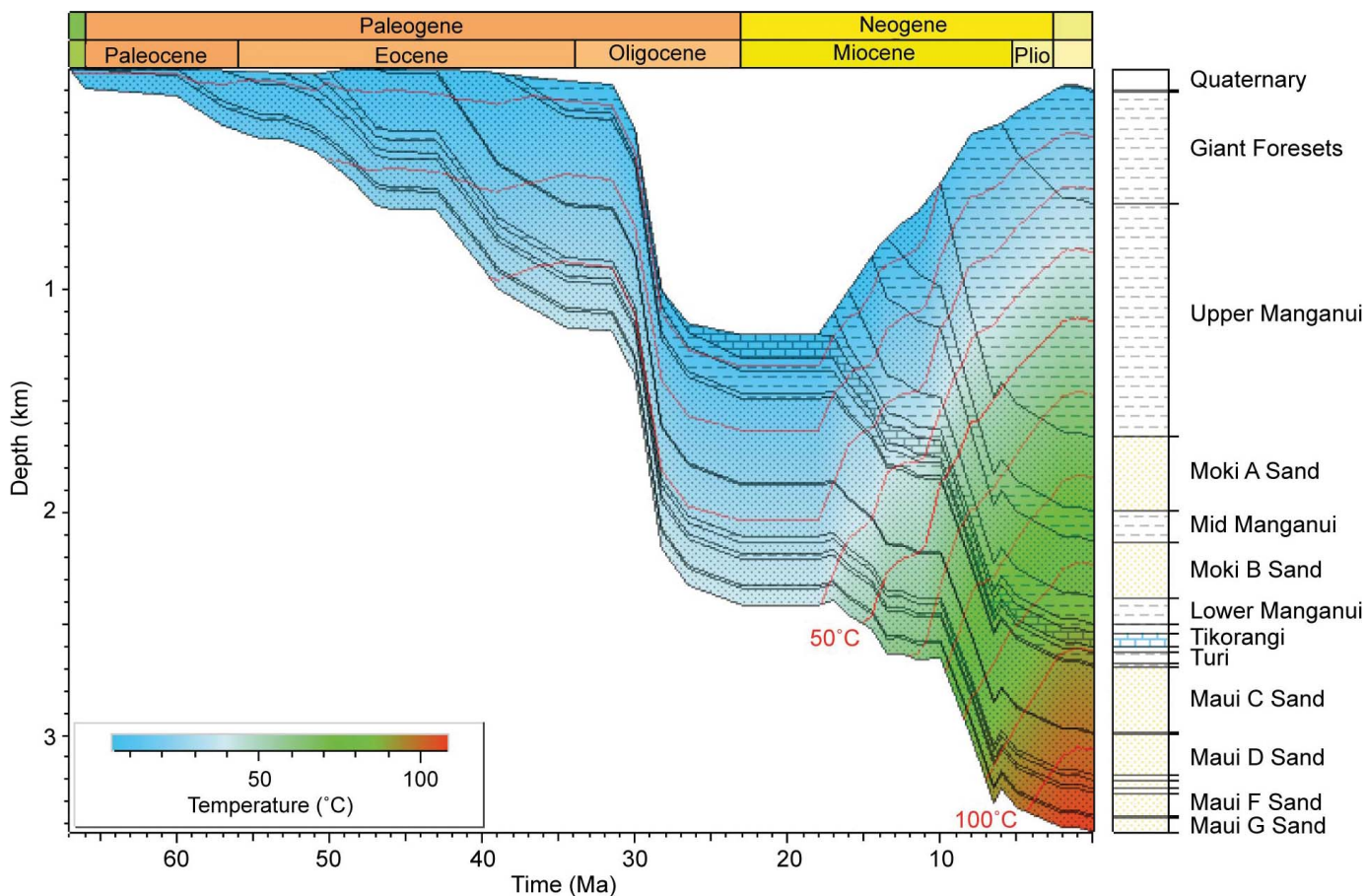
FIG. 11.—1D burial history plot of MB-R(1) (PetroMod). Red lines are isotherms (paleo-water depth adapted from Killops et al. (2009)).
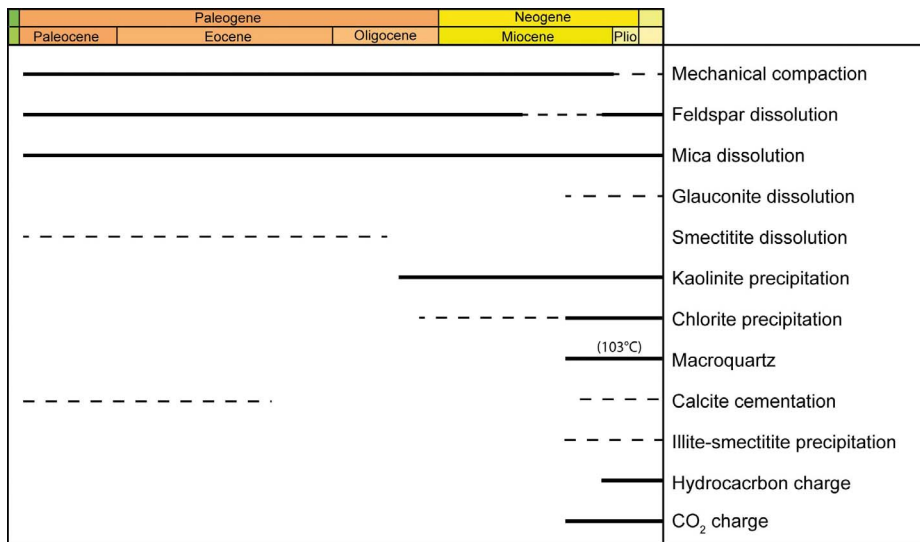
FIG. 12.—Diagenetic Paragenesis for F-Sands sandstone at the Maui Field (fluid-inclusion microthermometry after Killops et al. 2009).
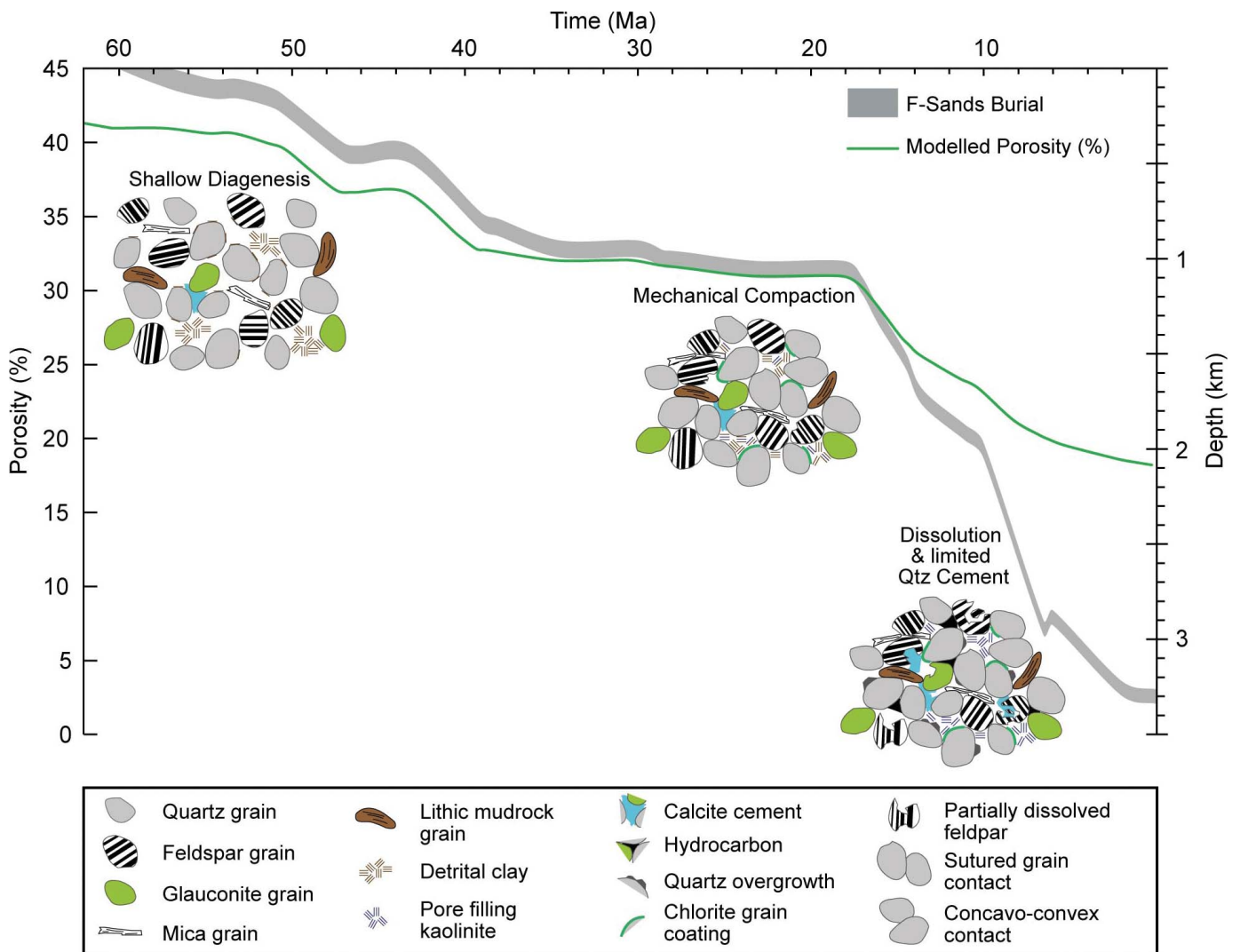

FIG. 13.—Plot of burial history and porosity development for the F-Sands in the Maui Field. Schematic thin-section micrographs displaying key features of diagenetic paragenesis during burial. Dissolution of feldspars has enhanced porosity with further quartz cementation restricted due to chlorite grain coatings and relatively late deeper burial of the F-Sands at the Maui Field.

pore waters, which can be associated with flushing of solutes derived from feldspar dissolution (e.g., Yuan et al. 2015a; Yuan et al. 2017). Ingression of meteoric water into the F-Sands reservoir may have occurred from late Eocene to early Oligocene (Figs. 11, 13; < 1 km burial depth) and following late Miocene uplift associated with the Cape Egmont Fault system (Fig. 4; Reilly et al. 2016). Significant leaching is likely to have occurred during shallow burial, leading to loss of dissolved solutes from the system, but subsequent rapid loading from 10 to 6 Ma (Fig. 13) would have rapidly increased effective stress and destroyed secondary porosity. The role played by meteoric fluids was important during shallow burial (< 1 km, late Eocene to early Oligocene), but during later stages of burial (since $\sim$ 10 Ma) CO_2 dissolved in pore fluids may have played a dominant role in the dissolution of the detrital grains and cement.

Cement Distribution and Heterogeneity

It might be expected that degradation of detrital feldspars in the predominantly arkosic F-Sands would have led to the precipitation of pervasive clay cement, but analyses using both reflected-light microscopy and SEM petrography have shown this not to be the case. It has been proposed that deep sandstone reservoirs (> 2 km) are geochemically closed systems, such that, at local scale, precipitation of cement equals its dissolution (Ehrenberg 1993; Higgs et al. 2007; Bjørlykke and Jahren 2012 Bjørlykke 2014). Higgs et al. (2013) proposed that a substantial percentage of the secondary minerals formed in Eocene formations in the Taranaki Basin have been precipitated in fine-grained heterolithic beds around coarser and well-sorted sandstone beds, for example in the Mangahewa and Kaimiro formations of the Kapuni Field. This implies a net redistribution of ions from coarse clean beds to fine heterolithic beds, a mechanism which could be invoked for the Maui Field F-Sands interval where fine to very fine-grained sandstone beds contain a significant percentage of clay cement (Fig. 8D) compared with interbedded coarser-grained high-permeability sandstone facies (Fig. 8B).

Fluid-inclusion analysis from the overlying D-Sands from Funnell et al. (2001) identify a late influx of gas-rich brine, characterized by clathrate-containing fluid inclusions, which is consistent with the formation of authigenic late-stage calcite cement. It could be expected that these brines may have flushed through the underlying F-Sands, leading to a proportion of the observed calcite cementation filling secondary porosity. As previously discussed, these brines can also be associated with high CO_2, which could lead to the dissolution and potentially reprecipitation of carbonate cements, further enhancing heterogeneity in the F-Sands.

CONCLUSIONS

1. Mechanical compaction has been the key mechanism for porosity reduction in the F-Sands of the Maui Field during their first 2500 m of burial, shown by grain fracturing, concavo-convex and quartz-to-quartz long grain contacts, deformed liable grains, and high COPL.

2. Dissolved CO_2 in pore fluids in the F-Sands of the Maui Field may have driven feldspar dissolution and enhanced secondary porosity (av. 1.7%) in the F-Sands.

3. Secondary porosity has been maintained due to a reduction in burial rates (from $\sim$ 6 Ma), thereby helping to prevent porosity loss via mechanical compaction.

4. The F-Sands display a limited amount of quartz cement because they entered the chemical compaction window (> 2500 m) only in the past 10 Ma and the significant quartz cementation realm $\sim$ 7 Ma. Quartz cement volumes are further controlled by chlorite grain coats which could play an important role in deeper sections of the Farewell Formation in the Taranaki Basin.

5. Dissolved solutes from CO_2-rich fluids in the F-Sand sandstones are preferentially precipitated in surrounding and interbedded fine-grained heterolithic siltstone beds. This process increases overall heterogeneity, leaving open pore throats and maintaining a primary intergranular porosity in sandstone reservoirs.

REFERENCES

Ambrose, W.A., Dutton, S.P., and Loucks, R.G., 2017, Depositional systems, facies variability, and their relationship to reservoir quality in the Jurassic Cotton Valley Group, Texas, Louisiana, and Mississippi onshore Gulf Coast: Gulf Coast Association of Geological Societies, Journal, v. 6, p. 21–46.

Armstrong, P.A., Allis, R.G., Funnell, R.H., and Chapman, D.S., 1998, Late Neogene exhumation patterns in Taranaki Basin (New Zealand): evidence from offset porosity-depth trends: Journal of Geophysical Research Solid Earth, v. 103, p. 30, 269–30, 282.

Athy, L.F., 1930, Density, porosity, and compaction of sedimentary rocks: American Association of Petroleum Geologists, Bulletin, v. 14, p. 1–24.

Barclay, S.A., and Worden, R.H., 2000, Geochemical modelling of diagenetic reactions in a sub-arkosic sandstone: Clay Minerals, v. 35, p. 57–67.

Bjørlykke, K., 1998, Clay mineral diagenesis in sedimentary basins: a key to the prediction of rock properties: examples from the North Sea Basin: Clay Minerals, v. 33, p. 15–34.

Bjørlykke, K., 2014, Relationships between depositional environments, burial history and rock properties. Some principal aspects of diagenetic process in sedimentary basins: Sedimentary Geology, v. 301, p. 1–14.

Bjørlykke, K., and Egeberg, P.K., 1993, Quartz cementation in sedimentary basins: American Association of Petroleum Geologists, Bulletin, v. 77, p. 1538–1548.

Bjørlykke, K., and Jahren, J., 2012, Open or closed geochemical systems during diagenesis in sedimentary basins: constraints on mass transfer during diagenesis and the prediction of porosity in sandstone and carbonate reservoirs: American Association of Petroleum Geologists, Bulletin, v. 96, p. 2193–2214.

Bull, S., Nicol, A., Strogen, D., Kroeger, K.F., and Seebeck, H.S., 2019, Tectonic controls on Miocene sedimentation in the Southern Taranaki Basin and implications for New Zealand plate boundary deformation: Basin Research, v. 31, p. 253–273.

Çağatay, M.N., Saner, S., Al-Saiyed, I., and Carrigan, W.J., 1996, Diagenesis of the Safaniya Sandstone Member (mid-Cretaceous) in Saudi Arabia: Sedimentary Geology, v. 105, p. 221–239.

Cao, Y., Yuan, G., Li, X., Wang, Y., Xi, K., Wang, X., Jia, Z., and Yang, T., 2014, Characteristics and origin of abnormally high porosity zones in buried Paleogene clastic reservoirs in the Shengtuo area, Dongying Sag, East China: Petroleum Science, v. 11, p. 346–362.

Chuhan, F.A., Kjeldstad, A., Bjørlykke, K., and Høeg, K., 2002, Porosity loss in sand by grain crushing: experimental evidence and relevance to reservoir quality: Marine and Petroleum Geology, v. 19, p. 39–53.

Chuhan, F.A., Kjeldstad, A., Bjørlykke, K., and Høeg, K., 2003, Experimental compression of loose sands: relevance to porosity reduction during burial in sedimentary basins: Canadian Geotechnical Journal, v. 1011, p. 995–1011.

Collen, J.D., and Newman, R.H., 1991, Porosity development in deep sandstones, Taranaki Basin, New Zealand: Journal of Southeast Asian Earth Sciences, v. 5, p. 449–452.

Crowhurst, P.V., Green, P.F., and Kamp, P.J.J., 2002, Appraisal of (U-Th)/He apatite thermochronology as a thermal history tool for hydrocarbon exploration: an example from the Taranaki Basin, New Zealand: American Association of Petroleum Geologists, Bulletin, v. 86, p. 1801–1819.

Dyson, I.A., 1998, Greensand reservoirs in siliciclastic shoreline systems: facies models for hydrocarbon exploration: Australian Petroleum Production and Exploration Association, Journal, v. 38, p. 132–144.

Ehrenberg, S.N., 1993, Preservation of anomalously high porosity in deeply buried sandstones by grain-coating chlorite: examples from the Norwegian continental shelf: American Association of Petroleum Geologists, Bulletin, v. 77, p. 1260–1286.

El Albani, A., Meunier, A., and Fürsich, F., 2005, Unusual occurrence of glauconite in a shallow lagoonal environment (Lower Cretaceous, northern Aquitaine Basin, SW France): Terra Nova, v. 17, p. 537–544.

ESTEBAN, M., AND TABERNER, C., 2003, Secondary porosity development during late burial in carbonate reservoirs as a result of mixing and/or cooling of brines: Journal of Geochemical Exploration, v. 78–79, p. 355–359.

FRANKS, S.G., AND FORESTER, R.W., 1984, Relationships among secondary porosity, pore-fluid chemistry and carbon dioxide, Texas Gulf Coast, *in* Mcdonald, D.A., and Surdam, R.C., eds., Clastic Diagenesis: American Association of Petroleum Geologists, v. 37, p. 63–79.

FUNNELL, R., CHAPMAN, D., ALLIS, R., AND ARMSTRONG, P., 1996, Thermal state of the Taranaki Basin, New Zealand: Journal of Geophysical Research, v. 101, p. 25,197–25,215.

FUNNELL, R.H., STAGPOOLE, V.M., NICOL, A., KILLOPS, S.D., REYES, A.G., AND DARBY, D., 2001, Migration of Oil and Gas into the Maui Field, Taranaki Basin, New Zealand, *in* Australian Petroleum Production and Exploration Association, Eastern Australasian Basins Symposium, p. 121–128.

FUNNELL, R., STAGPOOLE, V.M., NICOL, A., McCORMACK, N., AND REYES, A.G., 2004, Petroleum generation and implications for migration: a Maui Field charge study, Taranaki Basin: New Zealand Petroleum Conference, Proceedings, p. 1–9.

FURLONG, K.P., AND KAMP, P.J.J., 2013, Changes in plate boundary kinematics: punctuated or smoothly varying: evidence from the mid-Cenozoic transition from lithospheric extension to shortening in New Zealand: Tectonophysics, v. 608, p. 1328–1342.

GILES, M.R., INDRELID, S.L., BEYNON, G.V., AND AMTHOR, J., 2009, The origin of large-scale quartz cementation: evidence from large data sets and coupled heat–fluid mass transport modelling, *in* Worden, R., and Morad, S., eds., Quartz Cementation in Sandstones: The International Association of Sedimentologists, p. 21–38.

HAILE, B.G., KLAUSEN, T.G., CZARNIECKA, U., XI, K., JAHREN, J., AND HELLEVANG, H., 2018, How are diagenesis and reservoir quality linked to depositional facies? A deltaic succession, Edgeøya, Svalbard: Marine and Petroleum Geology, v. 92, p. 519–546.

HANSLEY, P.L., AND NUCCIO, V.F., 1992, Upper Cretaceous Shannon Sandstone reservoirs, Powder River Basin, Wyoming: evidence for organic acid diagenesis? American Association of Petroleum Geologists, Bulletin ,v. 76, p. 781–791.

HANTSCHEL, T., AND KAUERAUF, A.I., 2009, Fundamentals of Basin and Petroleum Systems Modeling: Berlin, Springer-Verlag, p. 476.

HIGGS, K.E., AND KING, P.R., 2018, Sandstone provenance and sediment dispersal in a complex tectonic setting: Taranaki Basin, New Zealand: Sedimentary Geology, v. 372, p. 112–139.

HIGGS, K.E., ZWINGMANN, H., REYES, A.G., AND FUNNELL, R.H., 2007, Diagenesis, porosity evolution, and petroleum emplacement in tight gas reservoirs, Taranaki Basin, New Zealand: Journal of Sedimentary Research, v. 77, p. 1003–1025.

HIGGS, K.E., KING, P.R., RAINE, J.I., SYKES, R., BROWNE, G.H., CROUCH, E.M., AND BAUR, J.R., 2012, Sequence stratigraphy and controls on reservoir sandstone distribution in an Eocene marginal marine–coastal plain fairway, Taranaki Basin, New Zealand: Marine and Petroleum Geology, v. 32, p. 110–137.

HIGGS, K.E., FUNNELL, R.H., AND REYES, A.G., 2013, Changes in reservoir heterogeneity and quality as a response to high partial pressures of CO2 in a gas reservoir, New Zealand: Marine and Petroleum Geology, v. 48, p. 293–322.

HIGGS, K.E., ARNOT, M.J., AND BRINDLE, S., 2015, Advances in grain-size, mineral, and pore-scale characterization of lithic and clay-rich reservoirs: American Association of Petroleum Geologists, Bulletin, v. 99, p. 1315–1348.

HOLT, W.E., AND STERN, T.A., 1994, Subduction, platform subsidence, and foreland thrust loading: the late Tertiary development of Taranaki Basin, New Zealand: Tectonics: v. 13, p. 1068–1092.

HOOD, S.D., NELSON, C.S., AND KAMP, P.J.J., 2003, Lithostratigraphy and depositional episodes of the Oligocene carbonate-rich Tikorangi Formation, Taranaki Basin, New Zealand: New Zealand Journal of Geology and Geophysics, v. 46, p. 363–386.

HOSSAIN, Z., FABRICIUS, I.L., AND CHRISTENSEN, H.F., 2009, Elastic and nonelastic deformation of greensand: The Leading Edge, v. 28, p. 86–88.

IVANOVSKAYA, T.A., GOR'KOVA, N.V., KARPOVA, G.V., POKROVSKAYA, E.V., AND DRITS, V.A., 2003, Chloritization of globular and platy phyllosilicates of the glauconite series in terrigenous rocks of the upper Riphean Päräjärvi Formation (Srednii Peninsula): Lithology and Mineral Resources, v. 38, p. 495–508.

KAMP, P.J.J., AND GREEN, P.F., 1990, Thermal and tectonic history of selected Taranaki Basin (New Zealand) wells assessed by apatite fission track analysis: American Association of Petroleum Geologists, Bulletin, v. 74, p. 1401–1419.

KILLOPS, S.D., REYES, A., AND FUNNELL, R.H., 2009, Filling history of the Maui B Field, New Zealand: new information from oil inclusions in authigenic minerals from the oil leg in the Maui-B1 well F Sands: Journal of Petroleum Geology, v. 32, p. 271–286.

KING, P.R., AND THRASHER, G.P., 1996, Cretaceous–Cenozoic Geology and Petroleum Systems of the Taranaki Basin, New Zealand: New Zealand: Institute of Geological and Nuclear Sciences, Monograph 13, Ministry of Economic Development, Petroleum Report 3224, 244 p.

LANSON, B., BEAUFORT, D., BERGER, G., BAUER, A., CASSAGNABÈRE, A., AND MEUNIER, A., 2002, Authigenic kaolin and illitic minerals during burial diagenesis of sandstones: a review: Clay Minerals, v. 37, p. 1–22.

LUNDEGARD, P.D., 1992, Sandstone porosity loss: a "big picture" view of the importance of compaction: Journal of Sedimentary Petrology, v. 62, p. 250–260.

LUNDEGARD, P.D., AND LAND, L.S., 1986, Carbon dioxide and organic acids: their role in porosity enhancement and cementation, Paleogene of the Texas Gulf Coast, *in* Gautier, D.L., ed., Roles of Organic Matter in Sediment Diagenesis: SEPM, Special Publication 38, p. 129–146.

MANSURBEG, H., MORAD, S., SALEM, A., MARFIL, R., EL-GHALI, M.A.K., NYSTUEN, J.P., CAJA, M.A., AMOROSI, A., GARCIA, D., AND LA IGLESIA, A., 2008, Diagenesis and reservoir quality evolution of Palaeocene deep-water, marine sandstones, the Shetland–Faroes Basin, British continental shelf: Marine and Petroleum Geology, v. 25, p. 514–543.

MARTIN, K.R., BAKER, J.C., HAMILTON, P.J., AND THRASHER, G.P., 1994, Diagenesis and reservoir quality of Palaeocene sandstones in the Kupe South Field, Taranaki Basin, New Zealand: American Association of Petroleum Geologists, Bulletin, v. 78, p. 624–643.

MAZZULLO, S.J., AND HARRIS, P.M., 1992, Mesogenetic dissolution: its role in porosity development in carbonate reservoirs: American Association of Petroleum Geologists, Bulletin, v. 76, p. 607–620.

MITCHELL, J.S., MACKAY, K.A., NEIL, H.L., MACKAY, E.J., PALLENTIN, A., AND NOTMAN, P., 2012, Undersea New Zealand, 1:5,000,000: National Institute of Water and Atmospheric Research Chart, Miscellaneous Series No. 92.

NZP&M, 2014, New Zealand Petroleum Basins, New Zealand Petroleum & Minerals. p. 104.

O'NEILL, S.R., JONES, S.J., KAMP, P.J.J., SWARBRICK, R.E., AND GLUYAS, J.G., 2018, Pore pressure and reservoir quality evolution in the deep Taranaki Basin, New Zealand: Marine and Petroleum Geology, v. 98, p. 815–835.

ODIN, G.S., 1988, Introduction to the study of green marine clays, *in* Odin, G.S., ed., Green Marine Clays: Amsterdam, Elsevier, Developments in Sedimentology, v. 45, p. 1–3.

ODIN, G.S., AND MATTER, A., 1981, De glauconiarum origine: Sedimentology, v. 28, p. 611–641.

PAXTON, S., SZABO, J., AJDUKIEWICZ, J., AND KLIMENTIDIS, R., 2002, Construction of an intergranular volume compaction curve for evaluating and predicting compaction and porosity loss in rigid-grain sandstone reservoirs: American Association of Petroleum Geologists, Bulletin, v. 86, p. 2047–2067.

POLLOCK, R.M., AND CROUCH, E., 2005, Correlation of Paleocene to Eocene sediments between Tui-1 and the Maui Field, offshore Taranaki, New Zealand: New Zealand Petroleum Report Series, PR 3009.

POLLOCK, R.M., REYES, A.G., AND SYKES, R., 2003, Petrographic and fluid inclusions analysis of Kapuni Group sandstones in Tui-1 well, Taranaki Basin: New Zealand Petroleum Report Series, PR2836.

PORTER, R.J., ROJAS, A.M., AND SCHLÜTER, M., 2018, The impact of heterogeneity on waterflood developments in clastic inner shelf reservoirs: an example from the Holland Greensand Member, Rotterdam Field, The Netherlands, *in* Kilhams, B., Kukla, P.A., Mazur, S., McKie, T., Mijnlieff, H.F., and van Ojik, K., eds., Mesozoic Resource Potential in the Southern Permian Basin: Geological Society of London, Special Publication 469, 457–477.

PRYOR, W.A., 1973, Permeability–porosity patterns and variations in some Holocene sand bodies: American Association of Petroleum Geologists, Bulletin, v. 57, p. 162–189.

RANGANATHAN, V., AND TYE, R.S., 1986, Petrography, diagenesis, and facies controls on porosity in Shannon Sandstone, Hartzog Draw Field, Wyoming: American Association of Petroleum Geologists, Bulletin, v. 70, p. 56–69

REILLY, C., NICOL, A., WALSH, J.J., AND SEEBECK, H., 2015, Evolution of faulting and plate boundary deformation in the Southern Taranaki Basin, New Zealand: Tectonophysics, v. 651, p. 1–18.

REILLY, C., NICOL, A., WALSH, J.J., AND KROEGER, K.F., 2016, Temporal changes of fault seal and early charge of the Maui Gas-condensate field, Taranaki Basin, New Zealand: Marine and Petroleum Geology, v. 70, p. 237–250.

SBPT, 1969, Maui-1 Well Resume: New Zealand Petroleum & Minerals, Petroleum Report Series PR 540.

SCHMIDT, V., AND McDONALD, D.A., 1979, The role of secondary porosity in the course of sandstone diagenesis, *in* Scholle, P.A., and Schluger, P.R., eds., Aspects of Diagenesis: SEPM, Special Publication 26, p. 175–207.

SCHULZ-ROJAHN, J.P., SEEBURGER, D.A., AND BEACHER, G.J., 2003, Application of glauconite morphology in geosteering and for on-site reservoir quality assessment in very fine-grained sandstones: Carnarvon Basin, Australia, *in* Worden, R.H., and Morad, S., eds., Clay Mineral Cements in Sandstones: International Association of Sedimentologists, p. 473–488.

SEEWALD, J.S., 2003, Organic–inorganic interactions in petroleum-producing sedimentary basins: Nature, v. 426, p. 327.

SEYBOLD, O.M., GREENSTREET, C.W., AND HAWTON, D.A., 1996, Reservoir management of the giant Maui gas/condensate field: New Zealand Petroleum Exploration Conference, Proceedings, p. 125–132.

SHIERS, M.N., HODGSON, D.M., AND MOUNTNEY, N.P., 2017, Response of a coal-bearing coastal-plain succession to marine transgression: Campanian Neslen Formation, Utah, U.S.A.: Journal of Sedimentary Research, v. 87, p. 168–187.

SLOT-PETERSEN, C., EIDESMO, T., WHITE, J., AND RUESLÄTTEN, H.G., 1998, NMR formation evaluation applications in a complex low-resistivity hydrocarbon reservoir: Society of Petrophysicists and Well Log Analysts, 39th Annual Logging Symposium, Proceedings, p. 14.

SMALE, D., MAUK, J.L., PALMER, J., SOONG, R., AND BLATTNER, P., 1999, Variations in sandstone diagenesis with depth, time, and space, onshore Taranaki wells, New Zealand: New Zealand Journal of Geology and Geophysics, v. 42, p. 137–154.

STAGPOOLE, V., AND NICOL, A., 2008, Regional structure and kinematic history of a large subduction back thrust: Taranaki Fault, New Zealand: Journal of Geophysical Research: Solid Earth, v. 113, p. 1–19.

STERN, T.A., AND DAVEY, F.J., 1990, Deep seismic expression of a foreland basin: Taranaki Basin, New Zealand: Geology, v. 18, p. 979–982.

STOS, 1993a, MB-R(1) Well Completion Report, Mau B Field, PML381012, Offshore Taranaki Basin: Petroleum Report Series No. 1912.

STOS, 1993b, MB-W(2) Well Completion Report, Mau B Field, PML381012, Offshore Taranaki Basin: Petroleum Report Series No. 1932.

STRICKER, S., AND JONES, S.J., 2016, Enhanced porosity preservation by pore fluid overpressure and chlorite grain coatings in the Triassic Skagerrak, Central Graben, North Sea, UK, in Armitage, P.J., Butcher, A.R., Churchill, J.M., Csoma, A.E., Hollis, C., Lander, R.H., Omma, J.E., and Worden, R.H., eds., Reservoir Quality of Clastic and Carbonate Rocks: Analysis, Modelling and Prediction: Geological Society of London, Special Publications 435, p. 321–341.

STRICKER, S., JONES, S.J., AND GRANT, N.T., 2016, Importance of vertical effective stress for reservoir quality in the Skagerrak Formation, Central Graben, North Sea: Marine and Petroleum Geology, v. 78, p. 895–909.

STROGEN, D.P., 2011, Paleogeographic synthesis of the Taranaki Basin and surrounds: Geological & Nuclear Sciences, Science Report 2010/53.

STROGEN, D.P., BLAND, K.J., BULL, S., FOHRMANN, M.F., SCOTT, G.P.L., AND ZHU, H., 2014a, Regional seismic transects of selected lines from Taranaki Basin: Geological & Nuclear Sciences, Data Series 7b.

STROGEN, D.P., BLAND, K.J., NICOL, A., AND KING, P.R., 2014b, Paleogeography of the Taranaki Basin region during the latest Eocene–early Miocene and implications for the total drowning of Zealandia: New Zealand Journal of Geology and Geophysics, v. 57, p. 110–127.

STROGEN, D.P., SEEBECK, H., NICOL, A., KING, P.R., AND CRET, E., 2017, Two-phase Cretaceous–Paleocene rifting in the Taranaki Basin region, New Zealand; implications for Gondwana break-up: Geological Society of London, Journal, v. 174, p. 929–946.

SYKES, R., ZINK, K.G., ROGERS, K.M., PHILLIPS, A., AND VENTURA, G.T., 2012, New and Updated Geochemical Databases for New Zealand Petroleum Samples, with Assessments of Genetic Oil Families, Source Age, Facies and Maturity: Geological & Nuclear Sciences, Science Consultancy Report 2012/37.

TRIPATHI, A.R.P., AND KAMP, P.J.J., 2008, Timing of initiation of reverse displacement on the Taranaki Fault, northern Taranaki Basin: constraints from the on land record (Oligocene Te Kuiti Group): Auckland, New Zealand Petroleum Conference, Proceedings, p. 1–19.

VONK, A.J., AND KAMP, P.J.J., 2008, The Late Miocene Southern and Central Taranaki Inversion Phase (SCTIP) and related sequence stratigraphy and paleogeography: New Zealand Petroleum Conference, Proceedings, p. 1–17.

WANG, X., WANG, X., HU, W., WAN, Y., CAO, J., LU, C., WANG, R., AND CUI, M., 2017, Supercritical CO_2-involved water–rock interactions at 85°C and partial pressures of 10–20 MPa: sequestration and enhanced oil recovery: Energy Exploration & Exploitation, v. 35, p. 237–258.

WINN, R.D., 1994, Shelf sheet-sand reservoir of the lower Cretaceous Greensand, North Celtic Sea Basin, offshore Ireland: American Association of Petroleum Geologists, Bulletin, v. 78, p. 1775–1789.

WORDEN, R.H., AND MORAD, S., 2009, Clay minerals in sandstones: controls on formation, distribution and evolution, in Worden, R.H., and Morad, S., eds., Clay Mineral Cements in Sandstones: International Association of Sedimentologists, p. 473–488.

XU, T., APPS, J.A., AND PRUESS, K., 2005, Mineral sequestration of carbon dioxide in a sandstone–shale system: Chemical Geology, v. 217, p. 295–318.

YUAN, G., CAO, Y., CLUYAS, J., LI, X., XI, K., WANG, Y., JIA, Z., SUN, P., AND OXTOBY, N.H., 2015a, Feldspar dissolution, authigenic clays, and quartz cements in open and closed sandstone geochemical systems during diagenesis: typical examples from two sags in Bohai Bay Basin, East China: American Association of Petroleum Geologists, Bulletin, v. 99, p. 2121–2154.

YUAN, G., CAO, Y., JIA, Z., GLUYAS, J., YANG, T., WANG, Y., AND XI, K., 2015b, Selective dissolution of feldspars in the presence of carbonates: the way to generate secondary pores in buried sandstones by organic CO_2: Marine and Petroleum Geology, v. 60, p. 105–119.

YUAN, G., CAO, Y., GLUYAS, J., AND JIA, Z., 2017, Reactive transport modeling of coupled feldspar dissolution and secondary mineral precipitation and its implication for diagenetic interaction in sandstones: Geochimica et Cosmochimica Acta, v. 207, p. 232–255.